Titanium Dioxide (TiO$_2$) Mesocrystals: Synthesis, Growth Mechanisms and Photocatalytic Properties

Boxue Zhang, Shengxin Cao, Meiqi Du, Xiaozhou Ye *, Yun Wang and Jianfeng Ye *

Department of Chemistry, College of Science, Huazhong Agricultural University, Wuhan 430070, China; bx1058779150@hotmail.com (B.Z.); shengxincao@hotmail.com (S.C.); dumeiqi@webmail.hzau.edu.cn (M.D.); wangyun@mail.hzau.edu.cn (Y.W.)

* Correspondence: xzye@mail.hzau.edu.cn (X.Y); jianfengye@mail.hzau.edu.cn (J.Y.); Tel.: +86-27-8728 4018 (J.Y.)

check for updates

Abstract: Hierarchical TiO$_2$ superstructures with desired architectures and intriguing physico-chemical properties are considered to be one of the most promising candidates for solving the serious issues related to global energy exhaustion as well as environmental deterioration via the well-known photocatalytic process. In particular, TiO$_2$ mesocrystals, which are built from TiO$_2$ nanocrystal building blocks in the same crystallographical orientation, have attracted intensive research interest in the area of photocatalysis owing to their distinctive structural properties such as high crystallinity, high specific surface area, and single-crystal-like nature. The deeper understanding of TiO$_2$ mesocrystals-based photocatalysis is beneficial for developing new types of photocatalytic materials with multiple functionalities. In this paper, a comprehensive review of the recent advances toward fabricating and modifying TiO$_2$ mesocrystals is provided, with special focus on the underlying mesocrystallization mechanism and controlling rules. The potential applications of as-synthesized TiO$_2$ mesocrystals in photocatalysis are then discussed to shed light on the structure–performance relationships, thus guiding the development of highly efficient TiO$_2$ mesocrystal-based photocatalysts for certain applications. Finally, the prospects of future research on TiO$_2$ mesocrystals in photocatalysis are briefly highlighted.

Keywords: TiO$_2$; photocatalysis; mesocrystals; synthesis; modification

1. Introduction

Semiconductor-based photocatalysis is well known to be one of the most effective approaches to alleviate the serious conundrums of global energy exhaustion, as well as environmental deterioration, by utilizing the inexhaustible solar energy [1–7]. Among various kinds of semiconductors, Titanium dioxide (TiO$_2$) is the most attractive one as a photocatalyst owing to its high photoreactivity, outstanding chemical stability, easy availability, and cheap price [8–15]. Despite tremendous efforts having been made toward the fabrication of TiO$_2$ materials, as well as the investigation of their photocatalytic properties, real applications of TiO$_2$ in photocatalysis are still largely hampered by the wide band gap of TiO$_2$ (e.g., 3.2 eV for anatase and brookite, 3.0 eV for rutile), which can merely absorb ultraviolet radiation (accounting for < 5% of solar light), and the fast recombination of photoinduced charge carriers, which leads to low quantum efficiency [16–21]. It is always a hot topic in the research area of materials chemistry and photocatalysis to manipulate the morphology and architecture of TiO$_2$ to achieve extended light response and facilitate photogenerated electron-hole separation, thus realizing remarkably enhanced photocatalytic activity in various applications [22–26].

Recently, it has been well demonstrated that building highly ordered superstructures from nanocrystal building blocks is very important for fabricating new materials and devices, as this kind of nanoparticle assembly can not only display properties and functions associated with individual

nanoparticles, but can also exhibit new collective properties and advanced tunable functions [27–32]. In particular, mesocrystals, a new type of ordered superstructure built from crystallographically oriented nanocrystal subunits, have drawn significant research interest since the concept of "mesocrystal" was first introduced in 2005 [33,34]. These unique ordered superstructures were initially identified from the studies of the structural characteristics and growth mechanisms of biominerals, and were proposed to be formed through a non-classical, particle-mediated growth process, namely, mesoscale transformation, rather than the conventional classical, atom/ion-mediated crystallization route (Figure 1). Subsequently, the mesocrystal concept evolved from the classical mesocrystals, which were generated via the aforementioned mesoscale transformation process, to all the hierarchical materials built from crystallographically oriented nanocrystal subunits regardless of the mechanism of formation. Despite the flourishing emergence of reports on the fabrication of mesocrystals, the history of mesocrystal synthesis is closely related to the continuous exploitation of mesocrystals with new compositions and the persistent development of synthetic procedures having advantages in terms of low cost, convenience in handling, and easiness in compositional and structural control [35–41].
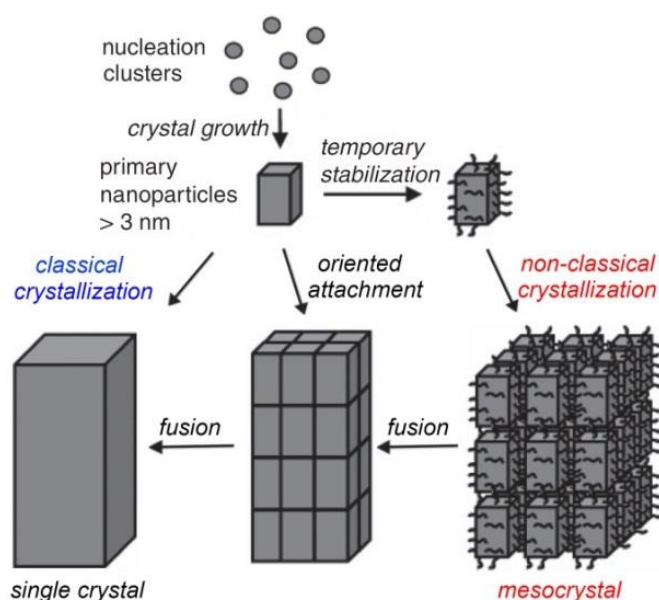

Figure 1. Schematic illustration of the single-crystal formation from classical crystallization, oriented attachment and non-classical crystallization. Reprinted with permission from [33]. Copyright John Wiley & Sons Inc., 2005.

To date, mesocrystals with a broad range of compositions involving metal oxides (e.g., TiO_2 [42–68], ZnO [69–85], Fe_2O_3 [86–95], CuO [96–101], SnOx [102,103], Co_3O_4 [104–108], Ag_2O [109]), metal chalcogenides (e.g., ZnS [110], PbS [111–113], Ag_2S [114], PbSe [115]), metals (e.g., Au [116–118], Ag [119], Cu [120], Pt [121,122], Pd [123]) have been produced, as introduced in some previous reviews [124–126]. Among these mesocrystals, TiO_2 mesocrystals are widely accepted to be particularly promising in photocatalytic applications [127–152]. It is noted that the high internal porosity and high surface areas of TiO_2 mesocrystals can be beneficial for the adsorption of reagents and provide more active sites for the subsequent photocatalytic reactions, while the well-oriented nanocrystal alignment provides effective conduction pathways and significantly enhances charge transport and separation with TiO_2 particles [135,153]. Although significant attention has been directed to fabricating TiO_2 mesocrystals with controlled morphologies, the realization of TiO_2 mesocrystals is always a challenging task, probably because the titanium precursors used are highly reactive, and it is rather difficult to precisely control the growth dynamic of TiO_2 crystals. Additionally, considering the wide band gap of the pristine TiO_2 materials, it is also demanding to modify the mesostructure of TiO_2

mesocrystals to realize broadened light absorption, thus achieving highly efficient photocatalysis in various applications.

In this review article, we first summarize numerous attempts toward the fabrication of TiO_2 mesocrystals. Four representative synthetic routes, namely, oriented topotactic transformation, growth on substrates, organic-additive-assisted growth in solution, and direct additive-free synthesis in solution, are presented one by one, with a special focus being channeled towards the underlying mesocrystallization mechanism and its controlling rules. The construction of doped TiO_2 mesocrystals, as well as TiO_2 mesocrystal-based heterostructures, is also covered in this review. The potential applications of the resultant TiO_2 mesocrystal-based materials in photocatalysis are then introduced to gain a deep understanding of the structure–performance relationships, thus providing useful guidelines for rationally designing and fabricating highly efficient TiO_2 mesocrystal-based photocatalysts for certain applications. Finally, some future research directions in the research area are briefly discussed and summarized.

2. Synthesis TiO_2 Mesocrystals

2.1. Oriented Topotactic Transformation

Early reports on the fabrication of TiO_2 mesocrystals were based on topotactic transformation from pre-synthesized NH_4TiOF_3 mesocrystals, as the titanium precursors used (e.g., $TiCl_4$, titanium tetrabutoxide (TBOT), titanium tetraisopropanolate (TTIP)) are normally highly reactive, making it rather challenging to manipulate the growth process of TiO_2 crystals upon direct syntheses. In 2007, O'Brien's group disclosed the first preparation of TiO_2 mesocrystals. In a synthetic procedure, NH_4TiOF_3 mesocrystals were first prepared in the $(NH_4)_2TiF_6$ and H_3BO_3 aqueous solution with the assistance of a nonionic surfactant (e.g., Brij 56, Brij 58, or Brij 700). After being washed with H_3BO_3 solution or sintered in air at 450 °C, the as-formed NH_4TiOF_3 mesocrystals were successfully transformed into anatase TiO_2 mesocrystals, with the original platelet-like shapes well preserved [42,43]. Such a topotactic transformation could proceed mainly because of the crystal structure similarity between NH_4TiOF_3 and anatase TiO_2 crystals (less than 0.02% in an average lattice mismatch), and the as-synthesized NH_4TiOF_3 mesocrystals could thus serve as a crystallographically matched template for the subsequent formation of TiO_2 mesocrystals (Figure 2). Owing to the great effectiveness of the methodology, NH_4TiOF_3 mesocrystals with a variety of morphologies were obtained by simply adjusting the reaction parameters, giving rise to a series of morphology-preserved anatase TiO_2 mesocrystals [44,45,137,141,143]. In addition, single-crystalline NH_4TiOF_3 crystals could also be utilized as a template for the oriented topotactic formation of anatase TiO_2 mesocrystals. For instance, by annealing a thin layer of aqueous solution containing TiF_4, NH_4F, and NH_4NO_3 on a Si wafer, nanosheet-shaped anatase TiO_2 mesocrystals enclosed by a high percentage of (001) facets were produced (Figure 3) [135]. Despite the one-step characteristic of the synthetic process, single-crystalline NH_4TiOF_3 nanosheets were actually first generated in the precursor solution at low annealing temperatures, which could then be easily transformed into anatase TiO_2 upon further increase in annealing temperature. With large quantities of N and F elements removed, the volume of the crystals decreased. Pores would form within the particles, resulting in anatase TiO_2 mesocrystals consisting of anatase nanocrystals predominantly enclosed by (001) facets.
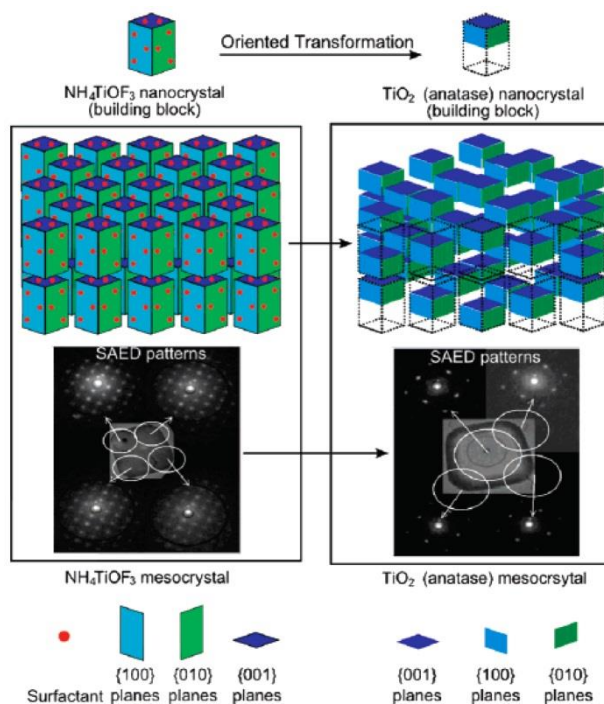
Figure 2. Schematic illustration of oriented topotactic transformation of NH_4TiOF_3 mesocrystal to anatase TiO_2 mesocrystal. The electron diffraction (SAED) patterns of the selected area illustrate single-crystal-like diffraction behavior for both samples. Reprinted with permission from [43]. Copyright American Chemical Society, 2008.
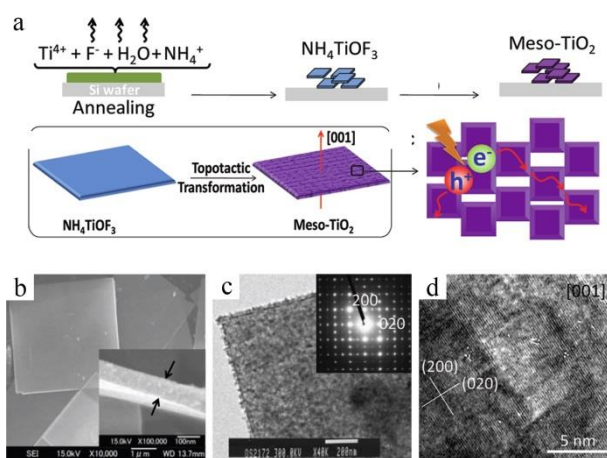

Figure 3. (**a**) Schematic presentation of oriented topotactic formation of anatase TiO_2 mesocrystals with dominant (001) facets; (**b**) SEM; (**c**) TEM; and (**d**) HRTEM images of anatase mesocrystals. The inset displays the related SAED pattern. Reprinted with permission from [135]. Copyright American Chemical Society, 2012.

Most recently, Qi's group proposed a new topotactic transformation method for fabricating anatase TiO_2 mesocrystals [154]. In their synthetic procedure, (010)-faceted orthorhombic titanium-containing precursor nanosheet arrays were firstly synthesized on conducting FTO glass substrate through solvothermally treating 0.1 M $K_2TiO(C_2O_4)_2$ in mixed solvents of deionized water and diethylene glycol. After a further hydrothermal treatment, the as-formed precursor nanosheet arrays could be readily converted to (001)-faceted anatase TiO_2 nanosheet arrays. It was revealed that the lattice match between the orthorhombic precursor crystal and the tetragonal anatase crystal accounted for the topotactic transformation from (010)-faceted precursor nanosheets to (001)-faceted anatase TiO_2 nanosheets (Figure 4).
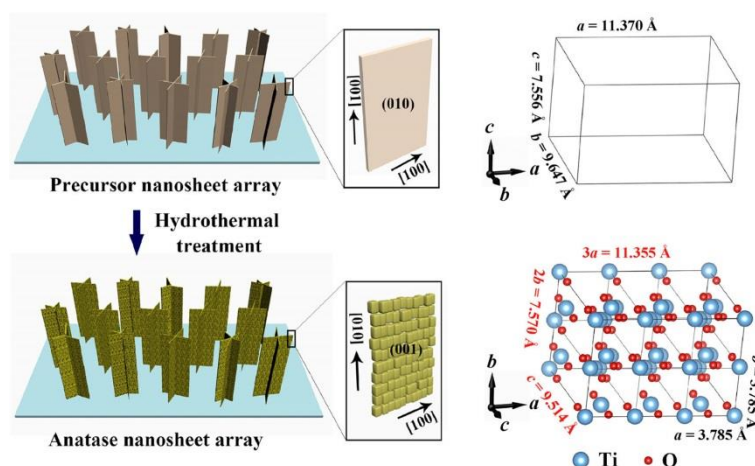
Figure 4. Schematic presentation of topotactic transformation from (010)-faceted precursor nanosheet arrays to (001)-faceted anatase TiO$_2$ nanosheet arrays on the basis of crystal lattice matchment between orthorhombic precursor crystal and tetragonal anatase crystal. Reprinted with permission from [154]. Copyright Springer, 2017.

2.2. Growth on Substrates

As presented above, topotactic transformation has been well demonstrated to be a very useful method to construct TiO$_2$ mesocrystals. However, precursors suitable for such a topotactic transformation are mainly limited to NH$_4$TiOF$_3$, and it is rather difficult to realize the morphological manipulation of the resultant TiO$_2$ mesocrystals at will. Therefore, it is highly desirable to explore facile solution-phase routes toward the direct fabrication of TiO$_2$ mesocrystals, since these kinds of syntheses are normally advantageous in light of their low cost, easy modulation of morphology, and great potential for environmentally benign production of inorganic materials. In 2008, Zeng's group first utilized multiwalled carbon nanotubes (CNTs) as substrate to grow anatase TiO$_2$ mesocrystals with controllable surface coverage [155]. It was revealed that the as-formed [001]-oriented petal-like anatase mesocrystals were uniformly distributed on CNTs, with TiO$_2$ nanocrystal building blocks having diameters in the range of 2–4 nm and mesopores having a very uniform size distribution centered at 2.5 nm. Additionally, by employing graphene nanosheets as a template to control the growth dynamic of TiO$_2$, uniform mesoporous anatase TiO$_2$ nanospheres were successfully generated and anchored on the graphene nanosheets (Figure 5) [156]. It is noteworthy that in comparison to the conventionally generated porous particles constructed by randomly aggregated anatase nanocrystals, the thus-formed mesoporous nanospheres were single-crystal-like. Detailed investigation on the growth process of the mesoporous anatase nanospheres revealed that such a graphene-nanosheet-assisted mesocrystallization route actually involved the nucleation of anatase TiO$_2$ on graphene nanosheets and subsequent oriented aggregation of tiny nanocrystals onto pre-anchored nuclei to reduce the total surface energy of anatase crystals. As a result, mesoporous mesocrystals of anatase TiO$_2$ would finally form. Moreover, Qi's group reported the fabrication of two-dimensional (2D) nanoarray structures constructed from mesocrystalline rutile TiO$_2$ nanorods on Ti substrate via a simple solution-phase synthesis [66]. These nanorod arrays were obtained by hydrothermally treating the aqueous solution of TBOT and HCl. It was revealed that during the growth process of the mesocrystalline rutile TiO$_2$ nanorod arrays, stem nanorods were first grown onto Ti substrate due to the high concentration of titanium-containing precursors, and with the consumption of the precursors, the resulting low concentration of reactant was responsible for the growth of the tiny nanotips with continuous crystal lattices, resulting in the final mesocrystalline rutile TiO$_2$ nanorods with a hierarchical architecture.
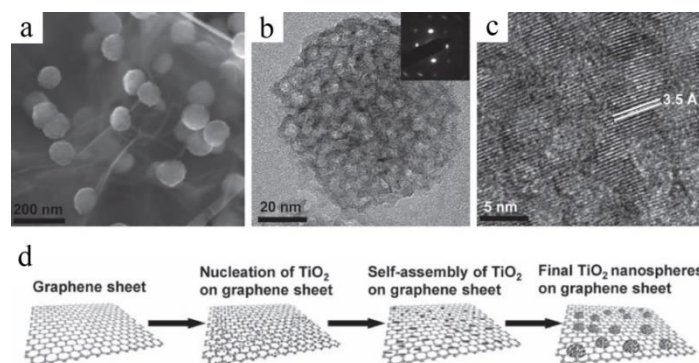
Figure 5. (**a**) SEM, (**b**) TEM, and (**c**) HRTEM images of mesoporous anatase TiO$_2$ nanospheres on graphene nanosheets. The inset is the SAED pattern related to a single nanosphere; (**d**) Schematic illustration of the growth mechanism of mesoporous anatase nanospheres. Reprinted with permission from [156]. Copyright John Wiley & Sons Inc., 2011.

2.3. Organic-Additive-Assisted Growth in Solution

Apart from the aforementioned solid templates or substrates, various organic additives could also be utilized to guide the formation of TiO$_2$ mesocrystals. In 2009, Yu's group first prepared hollow-sphere-shaped rutile TiO$_2$ mesocrystals assembled by nanorod subunits via a facile hydrothermal synthesis by using TiCl$_4$ as the titanium source and *N, N'*-dicyclohexylcarbodiimide (DCC) and L-serine as biological additives (Figure 6) [46]. It was proposed that such hollow-sphere-shaped mesocrystals were actually formed through a distinctive crystallization and transformation process, which involved the appearance of polycrystalline aggregates at the initial stage of reaction, mesoscale transformation to sector-shaped mesocrystals, further transformation of mesocrystals to nanorod bundles upon end-to-end and side-by-side oriented attachment accompanied by assembly of sectors to solid spheres, and final generation of hollow spheres via Ostwald ripening. Later on, with the assistance of organic small molecules of glacial acetic acid (HAc) and benzoic acid, rod-like anatase TiO$_2$ mesocrystals were successfully fabricated via a simple solvothermal route [127]. These mesocrystals were proposed to be formed through the well-known oriented attachment, and the mesocrystallization process was found to be carried out under the synergism of hydrophobic bonds, p-p interactions and "mixed-esters-templates". Furthermore, Gao's group synthesized spindle-shaped mesoporous anatase TiO$_2$ mesocrystals by utilizing peroxotitanium as the titanium source and polyacrylamide (PAM) as the polymer additive to adjust the growth process of TiO$_2$ [129]. They proposed that these anatase mesocrystals were formed via TiO$_2$-PAM co-assembly, accompanied by an amorphous-to-crystalline transformation.
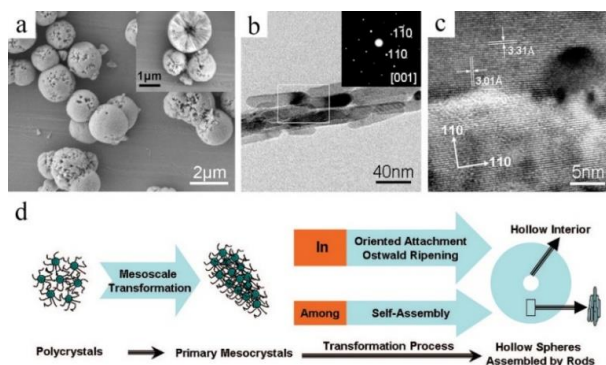

Figure 6. (**a**) SEM, (**b**) TEM, and (**c**) HRTEM images of hollow spheres of rutile TiO$_2$ mesocrystals. The inset in (**a**) is a magnified SEM image and the inset in (**b**) shows the related SAED pattern. (**d**) Schematic illustration of the formation mechanism of the rutile TiO$_2$ mesocrystals. Reprinted with permission from [46]. Copyright American Chemical Society, 2009.

In 2011, Tartaj's group developed a method based on inverse microemulsions to produce sub-100 nm sphere-like mesocrystalline nanostructures, which involved a two-stage temperature program [132]. In the first stage, the reaction at a low temperature (60 °C) triggered inverse microemulsions, resulting in thermal destabilization via forming nanomicellar structures smaller than 100 nm. The subsequent partial hydrolysis of $TiOSO_4$ produced sub-100-nm sphere-shaped TiO_2 frameworks through replicating those nanomicellar structures. In the second stage, increasing the reaction temperature to 80 °C or higher generated mesocrystalline TiO_2 architectures with interstitial porosity partially filled with surfactants. After the removal of the interstitial surfactants, mesoporosity was generated and uniform spherical-shaped mesocrystalline architectures of anatase TiO_2 with particle sizes ranging from 50 to 70 nm were produced finally. Later on, this method was extended to fabricate spherical-shaped mesoporous anatase TiO_2 mesocrystals with a much smaller size of 25 nm [133].

Recently, Zhao's group reported a facile evaporation-driven oriented assembly method to fabricate mesoporous anatase TiO_2 microspheres (~800 nm in diameter) with radially oriented hexagonal mesochannels and single-crystal-like pore walls (Figure 7) [64]. The synthesis started with the liquid-liquid phase separation, which was induced by the preferential evaporation of the solvent of tetrahydrofuran (THF) at a relatively low temperature (40 °C), and spherical-shaped PEO-PPO-PEO/TiO_2 oligomer composite micelles with PPO segments as the core and titania-associated PEO segments as the shell formed at the liquid-liquid phase interface. Upon further evaporation of THF at 40 °C, the concentration of the spherical micelles increased, leading to the formation of uniform mesoporous TiO_2 microspheres assembled by composite micelles (step 1 and 2). As the evaporation temperature increased to 80 °C, the continuous evaporation of the residual THF and hydrolyzed solvents from TBOT precursor drove the oriented growth of both mesochannels and nanocrystal building blocks from the initially formed spherical composite micelles along the free radial and restricted tangential direction within the TiO_2 microspheres (step 3). Radially oriented mesoporous anatase TiO_2 microspheres with single-crystal-like pore walls were produced after removal of the triblock copolymer templates finally (step 4). It is noteworthy that by simply adjusting the reaction parameters, mesoporous, single-crystal-like, olive-shaped, anatase TiO_2 mesocrystals constructed by ultrathin nanosheet subunits could also be synthesized [65].
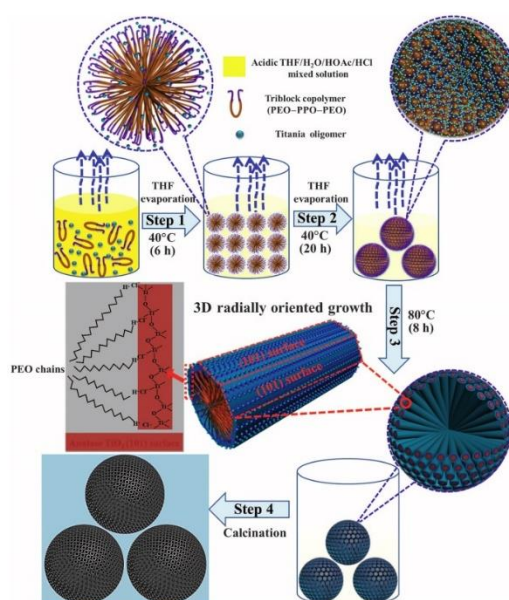

Figure 7. Schematic presentation of the formation process of mesoporous anatase TiO_2 microspheres with radially oriented hexagonal mesochannels and single-crystal-like pore walls through evaporation-driven oriented assembly. Reprinted with permission from [64]. Copyright American Chemical Society, 2015.

2.4. Direct Additive-Free Growth in Solution

Considering that the introduction of solid substrates or organic additives into the reaction system is unfavorable for the large-scale production of mesocrystals, it is, therefore, highly desirable to explore facile additive-free synthetic approaches toward functional mesocrystals with controllable crystallinity, porosity, morphology, and architecture. In 2011, Qi's group reported the first additive-free synthesis of nanoporous anatase TiO_2 mesocrystals with a spindle-shaped morphology, single-crystal-like structure, and tunable sizes via solvothermal treatment of the solution of TBOT in HAc, followed by calcination in air to remove the residual organics (Figure 8) [47]. These mesocrystals were illustrated to be elongated along the [001] direction, having lengths mainly in the range of 300–450 nm and diameters of 200–350 nm. It was revealed that under the solvothermal conditions, the reaction between TBOT and HAc firstly generated unstable titanium acetate complexes through ligand exchange/substitution, accompanied by the release of C_4H_9OH. The subsequent esterification reaction between thus-formed C_4H_9OH and the solvent HAc produced H_2O molecules slowly. Then, Ti-O-Ti bonds were formed via both nonhydrolytic-condensation and hydrolysis-condensation processes, resulting in transient amorphous fiber-like precursor. As the reaction continued, crystallized flower-like precursor was generated at the expense of the fiber-like precursor. This crystallized flower-like precursor acted as a reservoir to continuously release soluble titanium-containing species to generate tiny anatase nanocrystals. These tiny anatase nanocrystals underwent oriented aggregation along the [001] direction, together with some lateral attachment along some side facets of (101) facets, accompanied by the entrapment of in situ produced butyl acetate. As a result, [001]-elongated, spindle-shaped, anatase mesocrystals were produced when the reaction time was long enough. Further calcination in air would remove the butyl acetate residuals, consequently yielding nanoporous anatase TiO_2 mesocrystals.
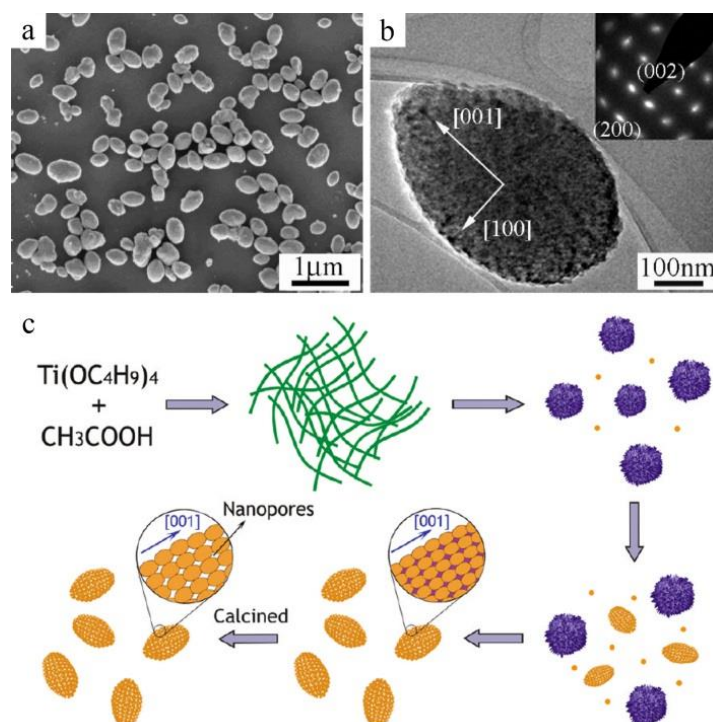

Figure 8. (**a**) SEM and (**b**) TEM images of nanoporous anatase TiO_2 mesocrystals obtained via solvothermal treatment of the solution of TBOT in HAc, followed by thermal treatment in air. The inset is the related SAED pattern of a single mesocrystal. (**c**) Proposed formation mechanism of nanoporous anatase TiO_2 mesocrystals. Reprinted with permission from [47]. Copyright American Chemical Society, 2011.

After half a month of Qi's pioneering work, Lu's group disclosed the fabrication of anatase TiO$_2$ mesocrystals with a single-crystal-like structure, high specific surface area, preferential exposure of highly reactive (001) crystal facets, and controllable mesoporous network [130]. As shown in Figure 9, by hydrothermal treating the solution of TiOSO$_4$ in *tert*-butyl alcohol, anatase TiO$_2$ nanocrystals were firstly generated, the (001) facets of which were preferably adsorbed by SO$_4^{2-}$ anions. Subsequent oriented attachment of the anatase nanocrystal building blocks created anatase clusters with the (001) facets well protected (step 1). Upon further attachment of the building blocks, anatase TiO$_2$ mesocrystals preferentially exposed by (001) facets and having a disordered mesoporous network were finally produced (step 2). It is noteworthy that when the growth was confined in a scaffold with ordered pore channels, such as mesoporous silica containing 2D (SBA-15, *P6mm* space group) and three-dimensional (3D) (KIT-6, *Ia3d* space group) ordered mesopores, the subsequent scaffold removal would lead to TiO$_2$ crystals with replicated 2D hexagonal (step 3) or 3D (step 4) ordered network structure, respectively. More interestingly, such a novel methodology could be extended to fabricating mesoporous single-crystal-like structures with other compositions (e.g., ZrO$_2$, CeO$_2$, etc.), thus providing promising materials for various applications.
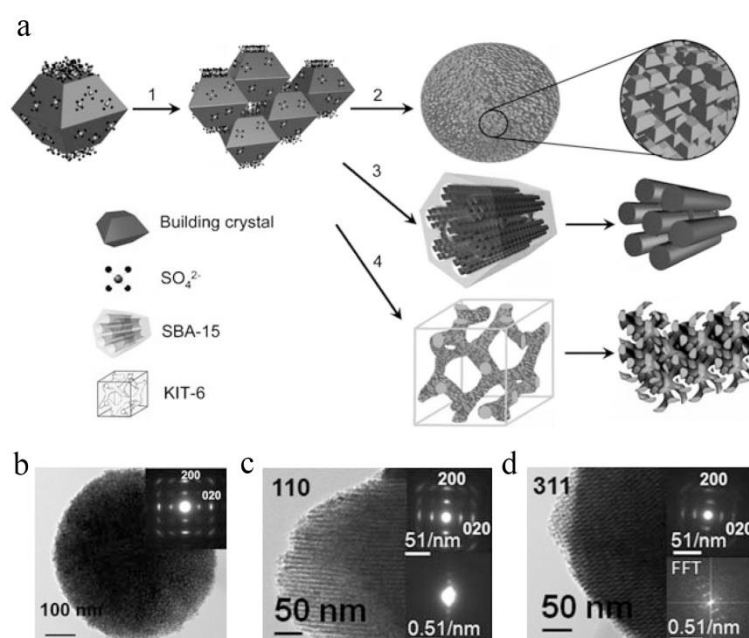

Figure 9. (**a**) Synthesis of mesoporous single-crystal-like anatase TiO$_2$ mesocrystals. (1) Formation of anatase clusters through oriented attachment of anatase nanocrystal building blocks with (001) facets preferably adsorbed by SO$_4^{2-}$ ions. (2) Further attachment of the building blocks resulting in mesocrystals with preferential exposed (001) facets and disordered mesoporous structure. Mesocrystals with ordered mesoporous structure were prepared by a confined growth of the anatase crystals in (3) SBA-15 (mesoporous silica with 2D ordered pore channels) and (4) KIT-6 (mesoporous silica with 3D ordered pore channels) followed by scaffold removal. TEM images of anatase mesocrystals with disordered mesopores (**b**), mesoporous mesocrystals grown within SBA-15 (**c**) and KIT-6 (**d**) followed by removal of the scaffold. The insets in (**b**–**d**) show the related SAED and FFT patterns. Reprinted with permission from [130]. Copyright John Wiley & Sons Inc., 2011.

The above two groups' fascinating work opened a promising avenue for the facile synthesis of porous anatase mesocrystals. An increasing number of reports of the direct fabrication of TiO$_2$ mesocrystals in solutions without any additives have been disclosed in recent years. For example, Leite's group proposed a kinetically controlled crystallization process to produce anatase TiO$_2$ mesocrystals with a truncated bipyramidal morphology, which was realized through a nonaqueous sol-gel reaction between TiCl$_4$ and *n*-octanol [131]. By adopting a similar method to adjust the hydrolysis dynamic of

TTIP in an oxalic acid aqueous solution, hierarchical rutile TiO$_2$ mesocrystals were produced [48]. Zhao's group developed a facile synthetic approach to fabricate regular shaped anatase TiO$_2$ mesocrystals with controllable proportion of (001) and (101) facets [136]. These anatase TiO$_2$ mesocrystals were prepared by solvothermally treating the solution of TTIP in formic acid (FA), and the exposed (101)/(001) ratio could be adjusted via simply varying the duration of solvothermal treatment. Most recently, our group proposed a novel synthetic procedure for producing spindle-shaped, single-crystal-like, anatase TiO$_2$ mesocrystals, which was realized by controlling the hydrolysis rate of TiCl$_3$ in the green solvent PEG-400 (Figure 10) [150]. These mesocrystals constructed by ultrafine nanocrystals (~1.5–4.5 nm in size) were revealed to be spindle-shaped and elongated along the [001] direction, having lengths predominantly of 50–85 nm and diameters of 20–40 nm. It was proposed that at the initial stage of the reaction, the chelation of PEG-400 to titanium centers firstly resulted in the formation of a titanium precursor. This chelated titanium precursor then underwent hydrolysis-condensation reaction in the presence of water to form Ti-O-Ti bonds, accompanied by the gradual oxidation of Ti^{3+} to Ti^{4+} by the dissolved oxygen, yielding numerous tiny anatase nanocrystals. These tiny anatase nanocrystals were temporarily stabilized by the solvent PEG-400 molecules and underwent oriented attachment along the [001] direction, together with some lateral attachment along some side facets of (101) facets, resulting in the formation of mesocrystalline anatase aggregates elongated along the [001] direction. It is worth noting that continuous oriented attachment of tiny anatase nanocrystals on the preformed elongated mesocrystalline aggregates occurred when reaction time was prolonged, and well-defined spindle-shaped anatase TiO$_2$ mesocrystals were produced when the reaction time was extended to 5 h.
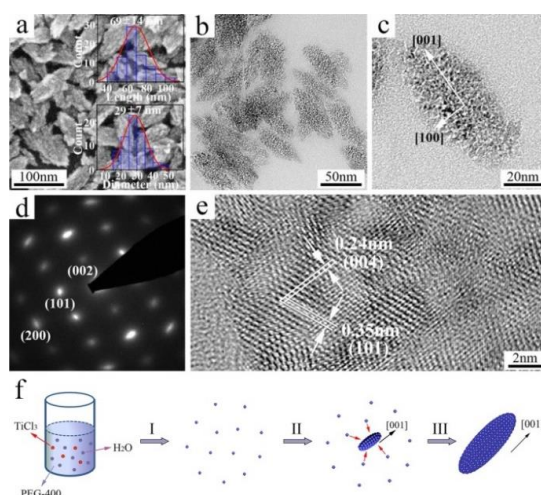

Figure 10. (**a**) SEM and (**b**,**c**) TEM images of anatase TiO$_2$ mesocrystals obtained via hydrolysis reaction of TiCl$_3$ in PEG-400. The insets in (**a**) are the related particle size distributions of the mesocrystals. (**d**) SAED pattern recorded on the anatase mesocrystal shown in (**c**); (**e**) HRTEM image of anatase mesocrystal; (**f**) A tentative mechanism for the formation of anatase mesocrystals. Reprinted with permission from [150]. Copyright American Chemical Society, 2017.

In addition to the widely employed titanium sources of TBOT, TTIP, TiOSO$_4$, and TiCl$_3$, it has been well proved that titanate precursors could also be utilized for the fabrication of TiO$_2$ mesocrystals. In 2012, Wei's group reported the synthesis of unique ultrathin-nanowire-constructed rutile TiO$_2$ mesocrystals through direct transformation from hydrogen titanate nanowire precursors (Figure 11) [61]. These hydrogen titanate nanowire precursors were prepared by hydrothermally treating the anatase TiO$_2$ in KOH solution, followed by acid washing. Then the precipitated hydrogen titanate nanowires were dispersed in HNO$_3$ aqueous solution and kept at 50 °C for 7 days, generating single-crystal-like rutile TiO$_2$ mesocrystals having lengths of about 300 nm and diameters 60–80 nm. It was proposed that such rutile mesocrystals were actually formed via face-to-face oriented attachment of ultrathin hydrogen titanate nanowire building blocks, accompanied by the conversion from hydrogen titanate precursor into rutile

TiO$_2$. To further modify the morphology of the rutile TiO$_2$ mesocrystals, Wei's group introduced the surfactant of sodium dodecyl benzene sulfonate (SDBS) into the reaction solution [62]. They found that SDBS played a vital role in the oriented self-assembly process, and rutile mesocrystals with controllable morphologies were successfully fabricated by varying the adding amount of SDBS. Specifically, uniform octahedral rutile TiO$_2$ mesocrystals 100–300 nm in size were obtained when the titanate/SDBS ratio was set at 0.09, while nanorod-shaped rutile TiO$_2$ mesocrystals were fabricated when the titanate/SDBS ratio increased to 0.15. Interestingly, the morphology and crystalline phase of the TiO$_2$ mesocrystals were demonstrated to be adjustable upon using different counterions to manipulate the growth dynamic of TiO$_2$ [63]. If the conversion of titanate nanowire precursors was carried out in HCl aqueous solution instead of HNO$_3$, dumbbell-shaped rutile TiO$_2$ superstructures composed of loose nanowire subunits were prepared, whereas anatase TiO$_2$ mesocrystals with a quasi-octahedral or truncated-octahedral morphology were obtained from H$_2$SO$_4$ aqueous solution. Such a novel synthetic procedure could also be extendable for the preparation of TiO$_2$ mesocrystals with other crystal phases. For example, by using amorphous titanates as titanium precursor and oxalic acid as structure-directing agent, novel brookite TiO$_2$ mesocrystals were successfully fabricated, as well [157].
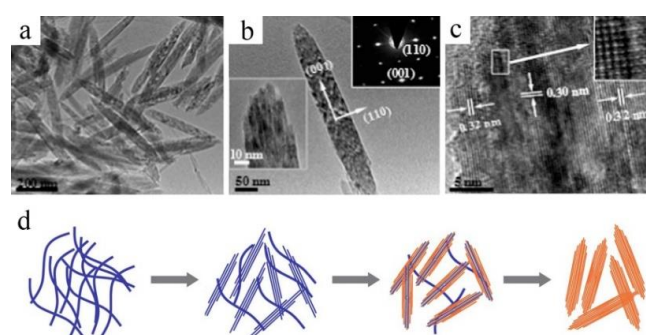

Figure 11. (**a**,**b**) TEM and (**c**) HRTEM images of rutile TiO$_2$ mesocrystals formed by conversion of titanate nanowire precursors in HNO$_3$ aqueous solution without any additives. The lower left inset in (**b**) is an enlarged TEM image, and the upper right inset is the SAED pattern related to the whole particle. (**d**) Schematic illustration of a tentative mechanism for the formation of rutile TiO$_2$ mesocrystals. Reprinted with permission from [61]. Copyright Royal Society of Chemistry, 2012.

3. Modification of TiO$_2$ Mesocrystals

3.1. Fabrication of Doped TiO$_2$ Mesocrystals

As mentioned above, the pristine TiO$_2$ can merely absorb ultra-violet irradiation owing to its wide band gap; continuous efforts have thus been channeled towards developing visible-light-responsive TiO$_2$ photocatalysts for various applications [8–13,16–21]. In addition to the well-known dye sensitization, the modification of TiO$_2$ with impurity doping was demonstrated to exhibit visible-light-responsive photocatalytic reactivity and showed improved stability upon light irradiation [11,16,19]. Considering the novel structural characteristics of TiO$_2$ mesocrystals, the fabrication of metal- or nonmetal-doped TiO$_2$ mesocrystals may give rise to ideal photocatalysts for particle applications, and thus has drawn considerable research interest [158–161]. For example, Majima's group successfully prepared N-doped anatase TiO$_2$ mesocrystals by solvothermal treatment of the pre-synthesized TiO$_2$ mesocrystals with triethanolamine [158]. Owing to the high internal porosity and high specific surface area of TiO$_2$ mesocrystals, the element of N could diffuse into the pores easily and was adsorbed on the surface. In addition, by stirring TiO$_2$ mesocrystals in NaF aqueous solution at room temperature, F-doped anatase TiO$_2$ mesocrystals could also be fabricated. It was proposed that surface fluorination via ligand exchange between F$^-$ and surface OH groups on TiO$_2$ occurred during the stirring process, resulting in the incorporation of F into TiO$_2$ mesocrystals. Combining these two doping strategies together would lead to the formation of N, F-codoped anatase TiO$_2$ mesocrystals without changing the morphology,

crystallinestructure, and surface area of TiO_2 mesocrystals (Figure 12). Apart from the nonmetal-doped TiO_2 mesocrystals, it was demonstrated that metal-doped TiO_2 mesocrystals could also be synthesized. Wei's group prepared pure rutile TiO_2 mesocrystals first, and then hydrothermally treated them in aqueous niobium oxalate solution. After a certain period of hydrothermal treatment, homogeneous Nb-doped rutile TiO_2 mesocrystals could finally be produced [161].
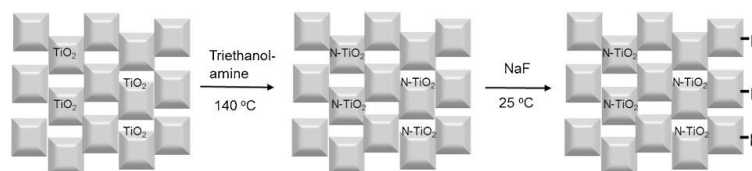

Figure 12. Proposed synthetic route toward N, F-codoped anatase TiO_2 mesocrystals. Reprinted with permission from [158]. Copyright Elsevier, 2016.

Recently, the introduction of oxygen vacancies or Ti^{3+} ions into TiO_2 to produce oxygen-deficient/Ti^{3+} self-doped TiO_2 mesostructures has been well accepted to be one of the most efficient ways to extend the light absorption region of TiO_2 to visible light [162–166]. Different from traditional doping strategies, introducing oxygen vacancies or Ti^{3+} ions is a unique doping method that can maintain the characteristic nature of TiO_2. At the same time, this kind of doping also improves the electroconductivity of TiO_2, thereby facilitating charge transportation within TiO_2 particles [162,164,167]. In this regard, great efforts have been made toward preparing oxygen-deficient/Ti^{3+} self-doped TiO_2 mesocrystals [65,136,150,168]. A good example in this area is that Zhao's group reported a facile evaporation-driven oriented assembly route combined with post thermal treatment in N_2 atmosphere to fabricate ultrathin-nanosheet-assembled olive-shaped mesoporous anatase TiO_2 mesocrystals (Figure 13) [65]. These mesoporous mesocrystals were illustrated to have high surface area (~189 m^2/g), large pore volume (0.56 cm^3/g), and abundant oxygen vacancies or unsaturated Ti^{3+} sites. Additionally, by thermally treating the anatase TiO_2 mesocrystals precipitated from the PEG-400/$TiCl_3$ mixed solution in vacuum, our group successfully synthesized Ti^{3+} self-doped, single-crystal-like, spindle-shaped, anatase TiO_2 mesocrystals [150]. Moreover, by reducing the pre-synthesized TiO_2 mesocrystals with $NaBH_4$, oxygen-deficient sheet-like anatase TiO_2 mesocrystals were also synthesized [168].
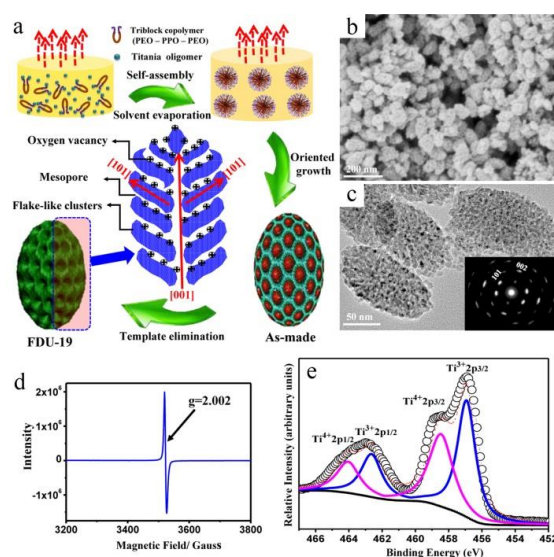

Figure 13. (**a**) Schematic illustration of the growth process of Ti^{3+} self-doped olive-shaped mesoporous anatase TiO_2 mesocrystals through evaporation-driven oriented assembly process; (**b**) SEM image, (**c**) TEM image, (**d**) EPR spectra, and (**e**) Ti2p XPS core-level spectra of Ti^{3+} self-doped olive-shaped mesoporous anatase TiO_2 mesocrystals. The inset in (**c**) is the SAED pattern of an individual mesocrystal. Reprinted with permission from [65]. Copyright American Chemical Society, 2015.

3.2. Construction of TiO$_2$ Mesocrystal-Based Heterostructures

Apart from the above-mentioned doping strategies, the coupling of TiO$_2$ mesocrystals with appropriate foreign elements to construct TiO$_2$ mesocrystal-based heterostructures is considered to be another effective way to enhance the light absorbance capability as well as inhibit the photoinduced charge carrier recombination [17,18,21]. Hitherto, various kinds of foreign elements have been successfully utilized to modify anatase TiO$_2$ mesocrystals [59,60,169–183]. For example, Sun's group successfully fabricated spindle-like TiO$_2$/CdS composites by uniformly distributing CdS nanoparticles onto nanoporous anatase mesocrystals via the simple hydrothermal and hot-injection methods [170]. Bian's group produced CdS quantum dot (QD)-decorated anatase TiO$_2$ mesocrystals preferably enclosed by (001) facets via the facile solvothermal treatment of TiOSO$_4$ in *tert*-butyl alcohol, followed by modification with CdS QDs via a simple ion-exchange treatment [175]. Majima's group applied a simple photodeposition method to deposit noble metal (Au, Pt) nanoparticles onto the pre-synthesized sheet-like anatase TiO$_2$ mesocrystals and realized the fabrication of novel metal-semiconductor superstructure nanocomposites [169]. Similarly, by adopting by a facile impregnation method, they were also able to deposite Au nanoparticles onto TiO$_2$ mesocrystals and fabricate promising plasmonic photocatalysts [172]. Moreover, to broaden the light-responsive region of TiO$_2$ mesocrystals to near-infrared (NIR) light, they also loaded Au nanorods with controllable size and tunable surface plasmon resonance (SPR) band onto anatase TiO$_2$ mesocrystals through the well-known ligand exchange method [179]. It is noteworthy that in addition to the deposition of guest elements onto the pre-synthesized anatase TiO$_2$ mesocrystals, anatase TiO$_2$ mesocrystals with desired morphologies could also be grown on various kinds of substrates. Tang's group introduced graphene oxide (GO) nanosheets into the reaction solution of TBOT in HAc. They found that after a solvothermal treatment at elevated temperatures, spindle-shaped anatase TiO$_2$ mesocrystals were successfully grown on the reduced graphene nanosheets [171]. Later on, Lu's group dispersed a certain amount of graphene into the reaction system of TiOSO$_4$ in *tert*-butyl alcohol. Upon microwave treatment of the obtained suspension, anatase TiO$_2$ mesocages with a single-crystal-like structure were found to be evenly anchored on graphene nanosheets [59]. Most recently, our group demonstrated that through in situ growth of nanosized defective anatase TiO$_{2-x}$ mesocrystals (DTMCs) on g-C$_3$N$_4$ nanosheets (NSs), a novel 3D/2D DTMC/g-C$_3$N$_4$ NS heterostructure with tight interfaces could be formed (Figure 14) [183].
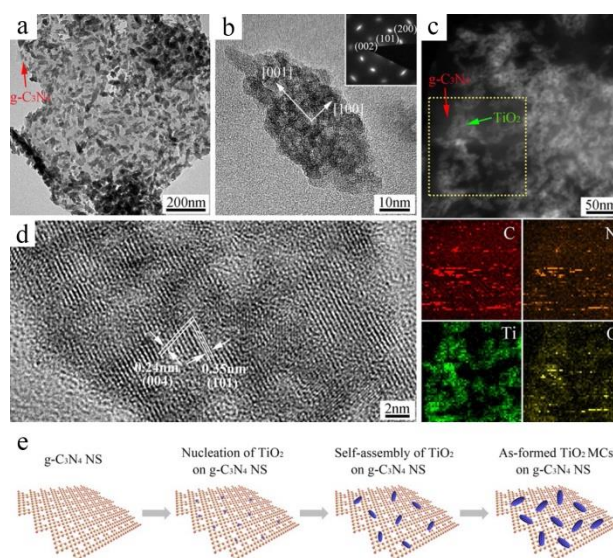

Figure 14. (**a**,**b**) TEM and (**c**) HRTEM images of 33.3% g-C$_3$N$_4$/DTMCs. The inset is the SAED pattern related to the whole particle. (**d**) HAADF-TEM image with elemental mapping of 33.3% g-C$_3$N$_4$/DTMCs. (**e**) Schematic presentation of the in situ growth of TiO$_2$ mesocrystals on a g-C$_3$N$_4$ nanosheet. Reprinted with permission from [183]. Copyright John Wiley & Sons Inc., 2018.

4. TiO$_2$ Mesocrystals for Photocatalytic Applications

4.1. Bare TiO$_2$ Mesocrystals for Photocatalytic Applications

Owing to the novel structural characteristics of mesocrystals, it is speculated the as-synthesized TiO$_2$ mesocrystals can be a promising candidate for photocatalytic applications. Liu's group first reported that the precipitated rod-like anatase TiO$_2$ mesocrystals delivered relatively higher photoreactivity toward the removal of methyl orange (MO) than the corresponding commercial P25 counterpart [127]. They ascribed the remarkably improved photocatalytic activity of the sample to its relatively high surface area, which could provide abundant sites for adsorption capability of MO. Yu's group proposed that the TiO$_2$ mesocrystals obtained in their additive-free reaction system possessed a well-crystallized rutile phase, low band gap energy and fast electron transfer property, and could exhibit high and stable photocatalytic activity for the removal of NO [128]. Lu's group evaluated the photoreactivity of the obtained single-crystal-like anatase TiO$_2$ mesocages and found that those unique TiO$_2$ mesocages with 3D ordered mesoporous channels exhibited superior photocatalytic activity toward oxidizing toluene to benzaldehyde and cinnamyl alcohol to cinnamaldehyde relative to that of TiO$_2$ mesocages with 2D ordered mesoporous channels, TiO$_2$ mesocages with disordered mesoporous channels, polycrystalline TiO$_2$, and P25 [130]. Leite's group claimed that the combination of high surface area and high crystallinity of the recrystallized mesocrystals can be more advantageous in photocatalytic applications than the corresponding disordered aggregate of nanocrystals [131].

Despite of the great efforts mentioned above toward the investigation of the photoreactivity of TiO$_2$ mesocrystals, it wasn't until 2012 that Majima's group first illustrated the photoelectronic properties of TiO$_2$ superstructures, in order to shed light on the intrinsic relationships between structural ordering and photoreactivity [135]. In their study, plate-like anatase TiO$_2$ mesocrystals synthesized via a topotactic transformation were selected as the target objects. These TiO$_2$ mesocrystals were built from crystallographically ordered anatase TiO$_2$ nanocrystal subunits and had a high surface area and high percentage of exposed highly reactive (001) facets. The photoconductive atomic force microscopy and time-resolved diffuse reflectance spectroscopy (DRS) were adopted to measure the charge transportation within the anatase mesocrystals, and the obtained results were compared with the reference anatase nanocrystals having similar surface area. It was consequently demonstrated that such a novel structure of anatase mesocrystals could exhibit largely enhanced charge separation and have remarkably long-lived charges, and thus could deliver greatly enhanced photoconductivity and photoreactivity (Figure 15). In 2015, Bian's group carefully evaluated the influence of intercrystal misorientation within anatase TiO$_2$ mesocrystals on the photoreactivity of the sample. They concluded that the misorientation of nanocrystal building blocks within anatase mesocrystals was harmful for the effective separation of photogenerated charge carriers and thus largely suppressed the photocatalytic efficiencies (Figure 16) [184]. Recently, Hu's group reported that the photocatalytic properties of anatase TiO$_2$ mesocrystals were actually largely dependent on the interfacial defects of intergrains within the particles [152]. They found that anatase TiO$_2$ mesocrystal photocatalysts exhibited much higher photocatalytic activity toward organic degradation and hydrogen evolution in comparison to single-crystalline crystals and poly crystalline crystals, which can be attributed to the presence of an appropriate number of interfacial defects at the intergrains and the facilitated charge carrier transport across the highly oriented interfaces. Moreover, it is inferred that the photoreactivity of the resultant anatase TiO$_2$ mesocrystal could be further optimized by regulation of defects, which could be simply achieved through annealing in redox atmospheres.
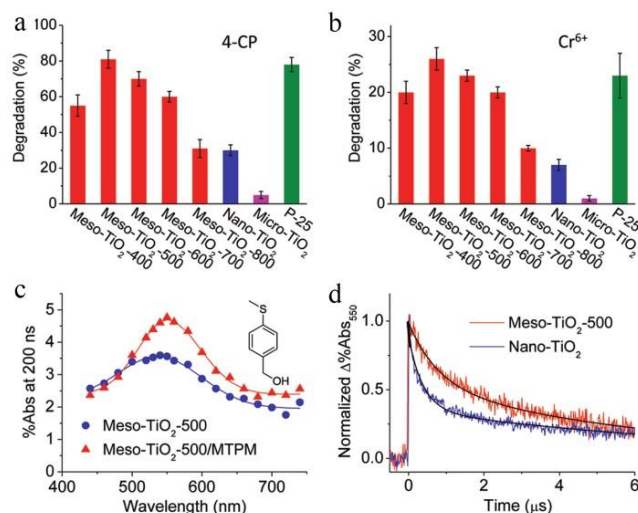
Figure 15. Photodegradation of (**a**) 4-CP and (**b**) Cr(VI) using various kinds of TiO$_2$ as catalysts. (**c**) Time-resolved diffuse reflectance spectra observed at 200 ns after the laser flash (355-nm) during the photolysis of Meso-TiO$_2$-500 in the absence and presence of 10 mM 4-(methylthio) phenyl methanol (MTPM) as the probe molecule to estimate the lifetime of the charge-separated state in acetonitrile. (**d**) Differential time traces of %Abs at 550 nm obtained in the presence of 10 mM MTPM for different TiO$_2$ samples in acetonitrile. Reprinted with permission from [135]. Copyright American Chemical Society, 2012.
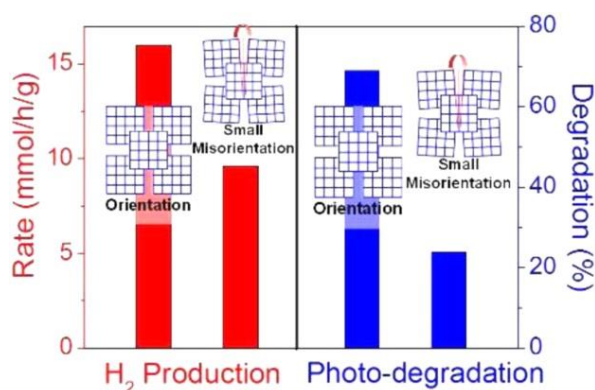

Figure 16. Rates comparison of phenol photodegradation and H$_2$ production upon TiO$_2$ mesocrystals built from well-ordered (red column) and less-ordered (blue column) orientation of nanocrystal subunits. Reprinted with permission from [184]. Copyright American Chemical Society, 2015.

4.2. Doped TiO$_2$ Mesocrystals for Photocatalytic Applications

Although a number of reports have demonstrated that TiO$_2$ mesocrystals can exhibit obviously enhanced photocatalytic performance in various applications, their real application is still hampered by the limited light absorbance of the pristine TiO$_2$ with a wide band gap. By utilizing the commonly used doping strategy, the thus-prepared doped TiO$_2$ mesocrystals can therefore become visible-light responsive, thus displaying enhanced visible-light-driven photoreactivity [136,150,158,159,168]. In 2016, Majima's group investigated the photoreactivity of N, F-codoped anatase TiO$_2$ mesocrystals. They found that, owing to the synergetic effect of N and F doping, the as-prepared product exhibited high visible-light-driven photoreactivity for degradating RhB and 4-nitrophenol (4-NP) [158]. Our group demonstrated that the obtained Ti^{3+} self-doped anatase TiO$_2$ mesocrystals showed much higher visible-light-driven photoreactivity toward removing NO and Cr (VI) compared with that of Ti^{3+} self-doped anatase nanocrystal counterparts. Such a photoreactivity enhancement was mainly due to the intrinsic self-doping nature, high crystallinity, as well as high porosity of the anatase

mesocrystals (Figure 17) [150]. Most recently, Majima's group applied femtosecond time-resolved DRS and single-particle photoluminescence (PL) measurements to characterize reduced TiO_2 mesocrystals to get deep understanding of the correlation between oxygen deficiency, photogenerated charge transfer, and photoreactivity of the material [168]. They confirmed the enhanced light absorption through forming oxygen vacancies did not always result in higher photoreactivity, and an appropriate amount of oxygen vacancies was required to improve the photogenerated charge carrier separation, thus giving rise to optimized photoreactivity.
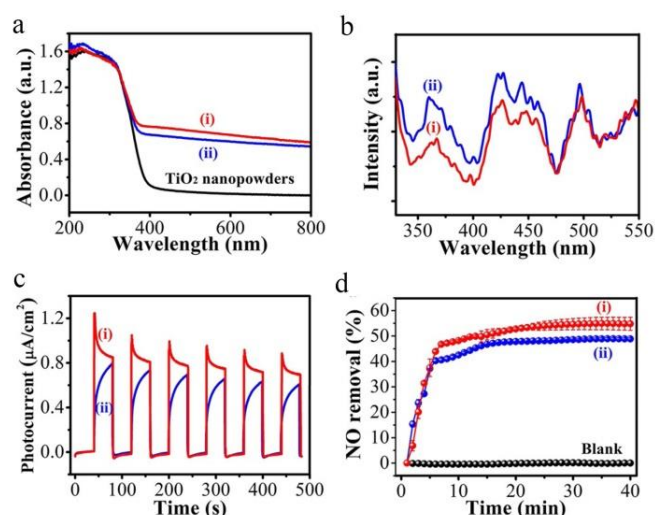

Figure 17. (**a**) UV-Vis DRS, (**b**) PL emission spectra, and (**c**) photocurrent intensity of (i) anatase mesocrystals and (ii) anatase nanocrystals of TiO_2 self-doped with Ti^{3+}. (**d**) Visible-light-driven photodegradation of NO upon (i) anatase mesocrystals and (ii) anatase nanocrystals self-doped with Ti^{3+}. Reprinted with permission from [150]. Copyright John Wiley & Sons Inc., 2017.

4.3. Composited TiO_2 Mesocrystals for Photocatalytic Applications

In addition to the aforementioned doping strategy, the coupling of TiO_2 mesocrystals with appropriate foreign materials to construct TiO_2-mesocrystal-based heterostructures is considered to be another useful methodology to broaden the light absorbance region of the material to visible light or even near-infrared (NIR) light, as well as to facilitate the mobility of photogenerated charge carriers within the particle [169–183]. For example, by utilizing CdS nanocrystals to modify spindle-shaped nanaporous anatase TiO_2 mesocrystals, Sun's group combined the advantages of the individual material, including (1) augmented specific surface area to provide more absorption and reactive sites; (2) TiO_2 mesocrystal substrate with high crystallinity and porosity to facilitate charge transport; (3) uniform distribution of CdS nanocrystals on mesocrystal surface and pores to facilitate charge transfer, and isolate photoinduced electrons and holes in two distinct materials; (4) tight contact between anatase mesocrystals and CdS nanocrystals to minimize the photo-corrosion and leaching off of CdS nanocrystals; and (5) extension of the photo-response of the material [170]. As expected, this unique spindle-shaped TiO_2/CdS photocatalyst exhibited relatively high visible-light-driven activity toward photodegradation of RhB. Bian's group reported that by decorating CdS QDs onto TiO_2 mesocrystals with a high percentage of exposed (001) facets, considerably high visible-light-driven photoreactivity could be achieved when selectively oxidizing various kinds of alcohols to their corresponding aldehydes [175]. Such an enhancement of the photoreactivity could be attributed to CdS QDs with improved photosensitization, porous mesostructure with high surface area, and exposed (001) facets with high surface energy and large quantities of oxygen vacancies, which could promote light absorbance in the visible light region, reactant molecule adsorption and activation, as well as photogenerated charge carrier separation. Majima's group claimed that superior electron transport and enhanced photoreactivity could be realized upon fabricating noble metal (Au, Pt)

nanoparticle-loaded nanoplate-shaped anatase TiO_2 mesocrystals [169]. They proposed that most of the photogenerated electrons could migrate from the dominant surface to the edge of the TiO_2 mesocrystal with the reduction reactions mainly occurring at its lateral surfaces containing (101) facets, as illustrated by single-molecule fluorescence spectroscopy. The as-fabricated metal-semiconductor nanocomposites were found to display significant enhancement of the photocatalytic reaction rate in organic degradation and hydrogen production. More interestingly, by utilizing Au nanorods to modify anatase TiO_2 mesocrystal superstructures, highly efficient photocatalytic hydrogen production under visible-NIR-light irradiation could be obtained [179]. This efficient hydrogen production could be attributed to the SPR of Au nanorods which injected electrons into anatase TiO_2 mesocrystals and the facilitated charge transport within mesocrystal particles. Apart from the adjustment of deposited guest particles, it was also demonstrated that efficient defect-state-induced hot electron transfer could be found in the as-prepared Au nanoparticles/reduced TiO_2 mesocrystal photocatalysts, which lead to the enhanced photoreactivity of the photocatalyst in removing methylene blue (MB) [182]. Most recently, our group evaluated the photoreactivity of the 3D/2D DTMC/g-C_3N_4 NS heterostructure with chemically bonded tight interfaces and found that the as-fabricated composite photocatalyst displayed much higher visible-light-driven photoreactivity toward removing the pollutants of MO and Cr(VI) than the corresponding DTMCs and g-C_3N_4 NSs counterparts (Figure 18) [183]. Systematic characterization results indicated that such an enhancement in the photoredox ability of the composite photocatalyst was based on the direct Z-scheme charge separation, as verified by the ·OH-trapping experiment.
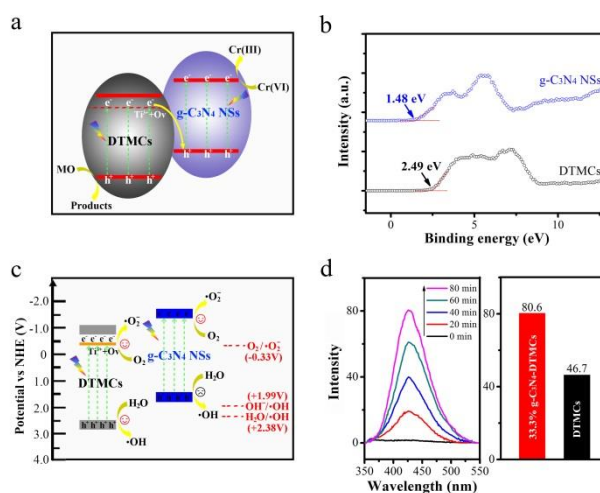

Figure 18. (**a**) Proposed Z-scheme charge-carrier transfer within DTMC/g-C_3N_4 composite. (**b**) XPS valence band spectra and (**c**) schematic electronic band structures of DTMCs and g-C_3N_4 NSs. (**d**) ·OH-trapping PL spectra of DTMCs/g-C_3N_4 and the corresponding fluorescence intensity upon DTMCs/g-C_3N_4 in comparison to DTMCs. Reprinted with permission from [183]. Copyright John Wiley & Sons Inc., 2018.

5. Summary and Outlook

In this paper, we have summarized some recent progress in fabricating TiO_2 mesocrystals, with special efforts being directed toward illustrating the underlying mesocrystallization process and its controlling rules. Four representative routes toward the fabrication of TiO_2 mesocrystals have been illustrated: oriented topotactic transformation, growth on substrates, organic-additive-assisted growth in solution, and direct additive-free synthesis in solution. In line with the flourishing emergence of reports on the fabrication of TiO_2 mesocrystals, the trends of TiO_2 mesocrystal synthesis are always related to the continuous exploitation of synthetic procedures having advantages like low cost, convenience in handling, and easiness of compositional and structural control. Apart from the fabrication of bare TiO_2 mesocrystals, the construction of doped TiO_2 mesocrystals, as well as TiO_2 mesocrystal-based heterostructures, are both considered to be promising strategies to further enhance

the performance of TiO_2 mesocrystals in various applications, and thus have also been covered in this review. Taking into account the novel structural characteristics of TiO_2 meoscrystals, such as high crystallinity, high porosity, and oriented nanocrystal assembly, the potential applications of the resultant TiO_2 mesocrystal-based materials in photocatalysis have been discussed to gain a deep understanding of the structure-performance relationships, which can provide useful guidelines for designing and fabricating highly efficient TiO_2 mesocrystal-based photocatalysts for certain applications.

Despite great success having been achieved in the fabrication of TiO_2 mesocrystals, the related mesocrystallization process of TiO_2 mesocrystals is still not fully understood, and deserves further investigation. It remains an ongoing task to figure out the specific reason for the well-ordered alignment of TiO_2 nanocrystal building blocks in certain circumstances and develop facile, reproducible, and environmentally benign synthetic approaches toward TiO_2 mesocrystals with desired morphologies and architectures. In addition, it should be pointed out that compared with the synthesis of TiO_2 mesocrystals, the application of thus-produced TiO_2 mesocrystals in photocatalysis is much less explored, suggesting the high demand of a deep investigation into TiO_2 mesocrystal-based photocatalysts in various applications. For example, although overall enhancement of photoctalytic activity of TiO_2 mesocrystals has been demonstrated in recent years, the real mechanism for the photoreactivity enhancement in certain applications has not yet been fully understood. It is a necessity to thoroughly examine the relationship between the structure and photocatalytic properties of TiO_2 mesocrystals, which can guide the rational design and fabrication of TiO_2 mesocrystals with desired morphologies and architectures to fully satisfy the needs of specific applications in the future. In addition, the exploration of TiO_2 mesocrystal-based photocatalysts in some more challenging application areas, such as selective CO_2 reduction, ammonia synthesis, and methanol activation, deserves significant research attention to fully excavate their potential in photocatalytic applications.

Author Contributions: J.Y. and X.Y. chose the topic; J.Y., X.Y., B.Z., S.C., M.D., and Y.W. wrote and revised the article.

Conflicts of Interest: The authors declare no conflict of interest.

References

1. Keane, D.A.; McGuigan, K.G.; Ibáñez, P.F.; Polo-López, M.I.; Byrne, J.A.; Dunlop, P.S.M.; O'Shea, K.; Dionysiou, D.D.; Pillai, S.C. Solar photocatalysis for water disinfection: Materials and reactor design. *Catal. Sci. Technol.* **2014**, *4*, 1211–1226. [CrossRef]

2. Spasiano, D.; Marotta, R.; Malato, S.; Fernandez-Ibanez, P.; Somma, I.D. Solar photocatalysis: Materials, reactors, some commercial and pre-industrialized applications. A comprehensive approach. *Appl. Catal. B Environ.* **2015**, *170–171*, 90–123. [CrossRef]

3. Chen, D.; Zhang, X.; Lee, A.F. Synthetic strategies to nanostructured photocatalysts for CO_2 reduction to solar fuels and chemicals. *J. Mater. Chem. A* **2015**, *3*, 14487–14516. [CrossRef]

4. Marszewski, M.; Cao, S.; Yu, J.; Jaroniec, M. Semiconductor-based photocatalytic CO_2 conversion. *Mater. Horiz.* **2015**, *2*, 261–278. [CrossRef]

5. Chen, S.; Takata, T.; Domen, K. Particulate photocatalysts for overall water splitting. *Nat. Rev. Mater.* **2017**, *2*, 17050. [CrossRef]

6. Zhu, S.; Wang, D. Photocatalysis: Basic principles, diverse forms of implementations and emerging scientific opportunities. *Adv. Energy Mater.* **2017**, *7*, 1700841. [CrossRef]

7. Christoforidis, K.C.; Fornasiero, P. Photocatalytic hydrogen production: A rift into the future energy supply. *ChemCatChem* **2017**, *9*, 1523–1544. [CrossRef]

8. Nakata, K.; Fujishima, A. TiO_2 photocatalysis: Design and applications. *J. Photochem. Photobiol. C Photochem. Rev.* **2012**, *13*, 169–189. [CrossRef]

9. Lan, Y.; Lu, Y.; Ren, Z. Mini review on photocatalysis of titanium dioxide nanoparticles and their solar applications. *Nano Energy* **2013**, *2*, 1031–1045. [CrossRef]
10. Schneider, J.; Matsuoka, M.; Takeuchi, M.; Zhang, J.; Horiuchi, Y.; Anpo, M.; Bahnemann, D.W. Understanding TiO$_2$ photocatalysis: Mechanisms and materials. *Chem. Rev.* **2014**, *114*, 9919–9986. [CrossRef]
11. Asahi, R.; Morikawa, T.; Irie, H.; Ohwaki, T. Nitrogen-doped titanium dioxide as visible-light-sensitive photocatalyst: Designs, developments, and prospects. *Chem. Rev.* **2014**, *114*, 9824–9852. [CrossRef] [PubMed]
12. Ma, Y.; Wang, X.; Jia, Y.; Chen, X.; Han, H.; Li, C. Titanium dioxide-based nanomaterials for photocatalytic fuel generations. *Chem. Rev.* **2014**, *114*, 9987–10043. [CrossRef] [PubMed]
13. Kapilashrami, M.; Zhang, Y.; Liu, Y.-S.; Hagfeldt, A.; Guo, J. Probing the optical property and electronic structure of TiO$_2$ nanomaterials for renewable energy applications. *Chem. Rev.* **2014**, *114*, 9662–9707. [CrossRef] [PubMed]
14. Wang, X.; Li, Z.; Shi, J.; Yu, Y. One-dimensional titanium dioxide nanomaterials: Nanowires, nanorods, and nanobelts. *Chem. Rev.* **2014**, *114*, 9346–9384. [CrossRef]
15. Li, W.; Wu, Z.; Wang, J.; Elzatahry, A.A.; Zhao, D. A perspective on mesoporous TiO$_2$ materials. *Chem. Mater.* **2014**, *26*, 287–298. [CrossRef]
16. Pelaez, M.; Nolan, N.T.; Pillai, S.C.; Seery, M.K.; Falaras, P.; Kontos, A.G.; Dunlop, P.S.M.; Hamilton, J.W.J.; Byrne, J.A.; O'Shea, K.; et al. A review on the visible light active titanium dioxide photocatalysts for environmental applications. *Appl. Catal. B Environ.* **2012**, *125*, 331–349. [CrossRef]
17. Park, H.; Park, Y.; Kim, W.; Choi, W. Surface modification of TiO$_2$ photocatalyst for environmental applications. *J. Photochem. Photobiol. C Photochem. Rev.* **2013**, *15*, 1–20. [CrossRef]
18. Zhang, G.; Kim, G.; Choi, W. Visible light driven photocatalysis mediated via ligand-to-metal charge transfer (LMCT): An alternative approach to solar activation of titania. *Energy Environ. Sci.* **2014**, *7*, 954–966. [CrossRef]
19. Etacheri, V.; Valentin, C.D.; Schneider, J.; Bahnemann, D.; Pillai, S.C. Visible-light activation of TiO$_2$ photocatalysts: Advances in theory and experiments. *J. Photochem. Photobiol. C Photochem. Rev.* **2015**, *25*, 1–29. [CrossRef]
20. Gao, M.; Zhu, L.; Ong, W.; Wang, J.; Ho, G.W. Structural design of TiO$_2$-based photocatalyst for H$_2$ production and degradation applications. *Catal. Sci. Technol.* **2015**, *5*, 4703–4726. [CrossRef]
21. Colmenares, J.C.; Varma, R.S.; Lisowski, P. Sustainable hybrid photocatalysts: Titania immobilized on carbon materials derived from renewable and biodegradable resources. *Green Chem.* **2016**, *18*, 5736–5750. [CrossRef]
22. Zhou, W.; Fu, H. Mesoporous TiO$_2$: Preparation, doping, and as a composite for photocatalysis. *ChemCatChem* **2013**, *5*, 885–894. [CrossRef]
23. Wang, M.; Ioccozia, J.; Sun, L.; Lin, C.; Li, Z. Inorganic-modified semiconductor TiO$_2$ nanotube arrays for photocatalysis. *Energy Environ. Sci.* **2014**, *7*, 2182–2202. [CrossRef]
24. Ola, O.; Maroto-Valer, M.M. Review of material design and reactor engineering on TiO$_2$ photocatalysis for CO$_2$ reduction. *J. Photochem. Photobiol. C Photochem. Rev.* **2015**, *24*, 16–42. [CrossRef]
25. Ge, M.; Li, Q.; Cao, C.; Huang, J.; Li, S.; Zhang, S.; Chen, Z.; Zhang, K.; Al-Deyab, S.S.; Lai, Y. One-dimensional TiO$_2$ nanotube photocatalysts for solar water splitting. *Adv. Sci.* **2017**, *4*, 1600152. [CrossRef]
26. Zhang, X.; Wang, Y.; Liu, B.; Sang, Y.; Liu, H. Heterostructures construction on TiO$_2$ nanobelts: A powerful tool for building high-performance photocatalysts. *Appl. Catal. B Environ.* **2017**, *202*, 620–641. [CrossRef]
27. Mann, S. Self-assembly and transformation of hybrid nano-objects and nanostructures under equilibrium and non-equilibrium conditions. *Nat. Mater.* **2009**, *8*, 781–792. [CrossRef] [PubMed]
28. Nie, Z.; Petukhova, A.; Kumacheva, E. Properties and emerging applications of self-assembled structures made from inorganic nanoparticles. *Nat. Nanotechnol.* **2010**, *5*, 15–25. [CrossRef]
29. Talapin, D.V.; Lee, J.-S.; Kovalenko, M.V.; Shevchenko, E.V. Prospects of colloidal nanocrystals for electronic and optoelectronic applications. *Chem. Rev.* **2010**, *110*, 389–458. [CrossRef]
30. Liu, J.-W.; Liang, H.-W.; Yu, S.-H. Macroscopic-scale assembled nanowire thin films and their functionalities. *Chem. Rev.* **2012**, *112*, 4770–4799. [CrossRef]
31. Klinkova, A.; Choueiri, R.M.; Kumacheva, E. Self-assembled plasmonic nanostructures. *Chem. Soc. Rev.* **2014**, *43*, 3976–3991. [CrossRef]
32. Cargnello, M.; Johnston-Peck, A.C.; Diroll, B.T.; Wong, E.; Datta, B.; Damodhar, D.; Doan-Nguyen, V.V.T.; Herzing, A.A.; Kagan, C.R.; Murray, C.B. Substitutional doping in nanocrystal superlattices. *Nature* **2015**, *524*, 450–455. [CrossRef] [PubMed]

33. Cölfen, H.; Antonietti, M. Mesocrystals: Inorganic superstructures made by highly parallel crystallization and controlled alignment. *Angew. Chem. Int. Ed.* **2005**, *44*, 5576–5591. [CrossRef] [PubMed]

34. Cölfen, H.; Antonietti, M. *Mesocrystals and Nonclassical Crystallization*; John Wiley & Sons: Chichester, UK, 2008.

35. Zhou, L.; O'Brien, P. Mesocrystals: A new class of solid materials. *Small* **2008**, *4*, 1566–1574. [CrossRef] [PubMed]

36. Song, R.-Q.; Cölfen, H. Mesocrystals-ordered nanoparticle superstructures. *Adv. Mater.* **2010**, *22*, 1301–1330. [CrossRef]

37. Fang, J.; Ding, B.; Gleiter, H. Mesocrystals: Syntheses in metals and applications. *Chem. Soc. Rev.* **2011**, *40*, 5347–5360. [CrossRef] [PubMed]

38. Zhou, L.; O'Brien, P. Mesocrystals-properties and applications. *J. Phys. Chem. Lett.* **2012**, *3*, 620–628. [CrossRef]

39. Uchaker, E.; Cao, G. Mesocrystals as electrode materials for lithium-ion batteries. *Nano Today* **2014**, *9*, 499–524. [CrossRef]

40. Tachikawa, T.; Majima, T. Metal oxide mesocrystals with tailored structures and properties for energy conversion and storage applications. *NPG Asia Mater.* **2014**, *6*, e100. [CrossRef]

41. Bergström, L.; Sturm (née Rosseeva), E.V.; Salazar-Alvarez, G.; Cölfen, H. Mesocrystals in biominerals and colloidal arrays. *Acc. Chem. Res.* **2015**, *48*, 1391–1402. [CrossRef]

42. Zhou, L.; Boyle, D.S.; O'Brien, P. Uniform NH_4TiOF_3 mesocrystals prepared by an ambient temperature self-assembly process and their topotaxial conversion to anatase. *Chem. Commun.* **2007**, 144–146. [CrossRef]

43. Zhou, L.; Smyth-Boyle, D.; O'Brien, P. A facile synthesis of uniform NH_4TiOF_3 mesocrystals and their conversion to TiO_2 mesocrystals. *J. Am. Chem. Soc.* **2008**, *130*, 1309–1320. [CrossRef] [PubMed]

44. Feng, J.; Yin, M.; Wang, Z.; Yan, S.; Wan, L.; Li, Z.; Zou, Z. Facile synthesis of anatase TiO_2 mesocrystal sheets with dominant {001} facets based on topochemical conversion. *CrystEngComm* **2010**, *12*, 3425–3429. [CrossRef]

45. Inoguchi, M.; Afzaal, M.; Tanaka, N.; O'Brien, P. The poly(ethylene glycol) assisted preparation of NH_4TiOF_3 mesocrystals and their topotactic conversion to TiO_2. *J. Mater. Chem.* **2012**, *22*, 25123–25129. [CrossRef]

46. Liu, S.-J.; Gong, J.-Y.; Hu, B.; Yu, S.-H. Mesocrystals of rutile TiO_2: Mesoscale transformation, crystallization, and growth by a biologic molecules-assisted hydrothermal process. *Cryst. Growth Des.* **2009**, *9*, 203–209. [CrossRef]

47. Ye, J.; Liu, W.; Cai, J.; Chen, S.; Zhao, X.; Zhou, H.; Qi, L. Nanoporous anatase TiO_2 mesocrystals: Additive-free synthesis, remarkable crystalline-phase stability, and improved lithium insertion behavior. *J. Am. Chem. Soc.* **2011**, *133*, 933–940. [CrossRef] [PubMed]

48. Wang, H.; Liu, Y.; Liu, Z.; Xu, H.; Deng, Y.; Shen, H. Hierarchical rutile TiO_2 mesocrystals assembled by nanocrystals-oriented attachment mechanism. *CrystEngComm* **2012**, *14*, 2278–2282. [CrossRef]

49. Zhen, M.; Guo, X.; Gao, G.; Zhou, Z.; Liu, L. Rutile TiO_2 nanobundles on reduced graphene oxides as anode materials for Li ion batteries. *Chem. Commun.* **2014**, *50*, 11915–11918. [CrossRef]

50. Wang, H.; Sun, L.; Wang, H.; Xin, L.; Wang, Q.; Liu, Y.; Wang, L. Rutile TiO_2 mesocrystallines with aggregated nanorod clusters: Extremely rapid self-reaction of the single source and enhanced dye-sensitized solar cell performance. *RSC Adv.* **2014**, *4*, 58615–58623. [CrossRef]

51. Fu, X.; Wang, B.; Chen, C.; Ren, Z.; Fan, C.; Wang, Z. Controllable synthesis of spherical anatase mesocrystals for lithium ion batteries. *New J. Chem.* **2014**, *38*, 4754–4759. [CrossRef]

52. Zhou, Y.; Wang, X.; Wang, H.; Song, Y.; Fang, L.; Ye, N.; Wang, L. Enhanced dye-sensitized solar cells performance using anatase TiO_2 mesocrystals with the Wulff construction of nearly 100% exposed {101} facets as effective light scattering layer. *Dalton Trans.* **2014**, *43*, 4711–4719. [CrossRef] [PubMed]

53. Hong, Z.; Zhou, K.; Zhang, J.; Huang, Z.; Wei, M. Facile synthesis of rutile TiO_2 mesocrystals with enhanced sodium storage properties. *J. Mater. Chem. A* **2015**, *3*, 17412–17416. [CrossRef]

54. Amarilla, J.M.; Morales, E.; Sanz, J.; Sobrados, I.; Tartaj, P. Electrochemical response in aprotic ionic liquid electrolytes of TiO_2 anatase anodes based on mesoporous mesocrystals with uniform colloidal size. *J. Power Sources* **2015**, *273*, 368–374. [CrossRef]

55. Hong, Z.; Zhou, K.; Huang, Z.; Wei, M. Iso-oriented anatase TiO_2 mesocages as a high performance anode material for sodium-ion storage. *Sci. Rep.* **2015**, *5*, 11960. [CrossRef]

56. Wu, D.; Cao, K.; Wang, H.; Wang, F.; Gao, Z.; Xu, F.; Guo, Y.; Jiang, K. Tunable synthesis of single-crystalline-like TiO$_2$ mesocrystals and their application as effective scattering layer in dye-sensitized solar cells. *J. Colloid Interface Sci.* **2015**, *456*, 125–131. [CrossRef]

57. Wu, Q.; Yang, X.; Zhou, W.; Gao, Q.; Lu, F.; Zhuang, J.; Xu, X.; Wu, M.; Fan, H.J. "Isofacet" anatase TiO$_2$ microcages: Topotactic synthesis and ultrastable Li-ion storage. *Adv. Mater. Interfaces* **2015**, *2*, 1500210. [CrossRef]

58. Hong, Z.; Hong, J.; Xie, C.; Huang, Z.; Wei, M. Hierarchical rutile TiO$_2$ with mesocrystalline structure for Li-ion and Na-ion storage. *Electrochim. Acta* **2016**, *202*, 203–208. [CrossRef]

59. Le, Z.; Liu, F.; Nie, P.; Li, X.; Liu, X.; Bian, Z.; Chen, G.; Wu, H.B.; Lu, Y. Pseudocapacitive sodium storage in mesoporous single-crystal-like TiO$_2$-graphene nanocomposite enables high-performance sodium-ion capacitors. *ACS Nano* **2017**, *11*, 2952–2960. [CrossRef] [PubMed]

60. Peng, Y.; Le, Z.; Wen, M.; Zhang, D.; Chen, Z.; Wu, H.B.; Li, H.; Lu, Y. Mesoporous single-crystal-like TiO$_2$ mesocages threaded with carbon nanotubes for high-performance electrochemical energy storage. *Nano Energy* **2017**, *35*, 44–51. [CrossRef]

61. Hong, Z.; Wei, M.; Lan, T.; Jiang, L.; Cao, G. Additive-free synthesis of unique TiO$_2$ mesocrystals with enhanced lithium-ion intercalation properties. *Energy Environ. Sci.* **2012**, *5*, 5408–5413. [CrossRef]

62. Hong, Z.; Wei, M.; Lan, T.; Cao, G. Self-assembled nanoporous rutile TiO$_2$ mesocrystals with tunable morphologies for high rate lithium-ion batteries. *Nano Energy* **2012**, *1*, 466–471. [CrossRef]

63. Hong, Z.; Xu, Y.; Liu, Y.; Wei, M. Unique ordered TiO$_2$ superstructures with tunable morphology and crystalline phase for improved lithium storage properties. *Chem. Eur. J.* **2012**, *18*, 10753–10760. [CrossRef]

64. Liu, Y.; Che, R.; Chen, G.; Fan, J.; Sun, Z.; Wu, Z.; Wang, M.; Li, B.; Wei, J.; Wei, Y.; et al. Radially oriented mesoporous TiO$_2$ microspheres with single-crystal–like anatase walls for high-efficiency optoelectronic devices. *Sci. Adv.* **2015**, *1*, e1500166. [CrossRef]

65. Liu, Y.; Luo, Y.; Elzatahry, A.A.; Luo, W.; Che, R.; Fan, J.; Lan, K.; Al-Enizi, A.M.; Sun, Z.; Li, B.; et al. Mesoporous TiO$_2$ mesocrystals: Remarkable defects-induced crystallite-interface reactivity and their in situ conversion to single crystals. *ACS Cent. Sci.* **2015**, *1*, 400–408. [CrossRef] [PubMed]

66. Cai, J.; Ye, J.; Chen, S.; Zhao, X.; Zhang, D.; Chen, S.; Ma, Y.; Jin, S.; Qi, L. Self-cleaning, broadband and quasi-omnidirectional antireflective structures based on mesocrystalline rutile TiO$_2$ nanorod arrays. *Energy Environ. Sci.* **2012**, *5*, 7575–7581. [CrossRef]

67. Dai, H.; Zhang, S.; Hong, Z.; Li, X.; Xu, G.; Lin, Y.; Chen, G. Enhanced photoelectrochemical activity of a hierarchical-ordered TiO$_2$ mesocrystal and its sensing application on a carbon nanohorn support scaffold. *Anal. Chem.* **2014**, *86*, 6418–6424. [CrossRef]

68. Dai, H.; Zhang, S.; Gong, L.; Li, Y.; Xu, G.; Lin, Y.; Hong, Z. The photoelectrochemical exploration of multifunctional TiO$_2$ mesocrystals and its enzyme-assisted biosensing application. *Biosens. Bioelectron.* **2015**, *72*, 18–24. [CrossRef]

69. Li, Z.; Gessner, A.; Richters, J.-P.; Kalden, J.; Voss, T.; Kuebel, C.; Taubert, A. Hollow zinc oxide mesocrystals from an ionic liquid precursor (ILP). *Adv. Mater.* **2008**, *20*, 1279–1285. [CrossRef]

70. Liu, Z.; Wen, X.D.; Wu, X.L.; Gao, Y.J.; Chen, H.T.; Zhu, J.; Chu, P.K. Intrinsic dipole-field-driven mesoscale crystallization of core-shell ZnO mesocrystal microspheres. *J. Am. Chem. Soc.* **2009**, *131*, 9405–9412. [CrossRef]

71. Wu, X.L.; Xiong, S.J.; Liu, Z.; Chen, J.; Shen, J.C.; Li, T.H.; Wu, P.H.; Chu, P.K. Green light stimulates terahertz emission from mesocrystal microspheres. *Nat. Nanotechnol.* **2011**, *6*, 103–106. [CrossRef]

72. Distaso, M.; Klupp Taylor, R.N.; Taccardi, N.; Wasserscheid, P.; Peukert, W. Influence of the counterion on the synthesis of ZnO mesocrystals under solvothermal conditions. *Chem. Eur. J.* **2011**, *17*, 2923–2930. [CrossRef] [PubMed]

73. Distaso, M.; Segets, D.; Wernet, R.; Taylor, R.K.; Peukert, W. Tuning the size and the optical properties of ZnO mesocrystals synthesized under solvothermal conditions. *Nanoscale* **2012**, *4*, 864–873. [CrossRef]

74. Hosono, E.; Tokunaga, T.; Ueno, S.; Oaki, Y.; Imai, H.; Zhou, H.; Fujihara, S. Crystal growth process of single-crystal-like mesoporous ZnO through a competitive reaction in solution. *Cryst. Growth Des.* **2012**, *12*, 2923–2931. [CrossRef]

75. Liu, M.-H.; Tseng, Y.-H.; Greer, H.F.; Zhou, W.; Mou, C.-Y. Dipole field guided orientated attachment of nanocrystals to twin-brush ZnO mesocrystals. *Chem. Eur. J.* **2012**, *18*, 16104–16113. [CrossRef] [PubMed]

76. Sun, S.; Zhang, X.; Zhang, J.; Song, X.; Yang, Z. Unusual designated-tailoring on zone-axis preferential growth of surfactant-free ZnO mesocrystals. *Cryst. Growth Des.* **2012**, *12*, 2411–2418. [CrossRef]

77. Waltz, F.; Wissmann, G.; Lippke, J.; Schneider, A.M.; Schwarz, H.-C.; Feldhoff, A.; Eiden, S.; Behrens, P. Evolution of the morphologies of zinc oxide mesocrystals under the influence of natural polysaccharides. *Cryst. Growth Des.* **2012**, *12*, 3066–3075. [CrossRef]

78. Wang, H.; Xin, L.; Wang, H.; Yu, X.; Liu, Y.; Zhou, X.; Li, B. Aggregation-induced growth of hexagonal ZnO hierarchical mesocrystals with interior space: Nonaqueous synthesis, growth mechanism, and optical properties. *RSC Adv.* **2013**, *3*, 6538–6544. [CrossRef]

79. Wang, S.-S.; Xu, A.-W. Template-free facile solution synthesis and optical properties of ZnO mesocrystals. *Cryst. Eng. Commun.* **2013**, *15*, 376–381. [CrossRef]

80. Peng, Y.; Wang, Y.; Chen, Q.-G.; Zhu, Q.; Xu, A.W. Stable yellow ZnO mesocrystals with efficient visible-light photocatalytic activity. *CrystEngComm* **2014**, *16*, 7906–7913. [CrossRef]

81. Liu, J.; Hu, Z.-Y.; Peng, Y.; Huang, H.-W.; Li, Y.; Wu, M.; Ke, X.-X.; Tendeloo, G.V.; Su, B.-L. 2D ZnO mesoporous single-crystal nanosheets with exposed {0001} polar facets for the depollution of cationic dye molecules by highly selective adsorption and photocatalytic decomposition. *Appl. Catal. B Environ.* **2016**, *181*, 138–145. [CrossRef]

82. Liu, M.-H.; Chen, Y.-W.; Liu, X.; Kuo, J.-L.; Chu, M.-W.; Mou, C.-Y. Defect-mediated gold substitution doping in ZnO mesocrystals and catalysis in CO oxidation. *ACS Catal.* **2016**, *6*, 115–122. [CrossRef]

83. Wang, H.; Wang, C.; Chen, Q.; Ren, B.; Guan, R.; Cao, X.; Yang, X.; Duan, R. Interface-defect-mediated photocatalysis of mesocrystalline ZnO assembly synthesized in-situ via a template-free hydrothermal approach. *Appl. Surf. Sci.* **2017**, *412*, 517–528. [CrossRef]

84. Liu, M.-H.; Chen, Y.-W.; Lin, T.-S.; Mou, C.-Y. Defective mesocrystal ZnO-supported gold catalysts: Facilitating CO oxidation via vacancy defects in ZnO. *ACS Catal.* **2018**, *8*, 6862–6869. [CrossRef]

85. Liang, S.; Gou, X.; Cui, J.; Luo, Y.; Qu, H.; Zhang, T.; Yang, Z.; Yang, Q.; Sun, S. Novel cone-like ZnO mesocrystals with coexposed (10-11) and (000-1) facets and enhanced photocatalytic activity. *Inorg. Chem. Front.* **2018**, *5*, 2257–2267. [CrossRef]

86. Park, G.-S.; Shindo, D.; Waseda, Y.; Sugimoto, T. Internal structure analysis of monodispersed pseudocubic hematite particles by electron microscopy. *J. Colloid Interface Sci.* **1996**, *177*, 198–207. [CrossRef]

87. Ahniyaz, A.; Sakamoto, Y.; Bergström, L. Magnetic field-induced assembly of oriented superlattices from maghemite nanocubes. *Proc. Natl. Acad. Sci. USA* **2007**, *104*, 17570–17574. [CrossRef]

88. Fang, X.-L.; Chen, C.; Jin, M.-S.; Kuang, Q.; Xie, Z.-X.; Xie, S.-Y.; Huang, R.-B.; Zheng, L.-S. Single-crystal-like hematite colloidal nanocrystal clusters: Synthesis and applications in gas sensors, photocatalysis and water treatment. *J. Mater. Chem.* **2009**, *19*, 6154–6160. [CrossRef]

89. An, Z.; Zhang, J.; Pan, S.; Yu, F. Facile template-free synthesis and characterization of elliptic a-Fe$_2$O$_3$ superstructures. *J. Phys. Chem. C* **2009**, *113*, 8092–8096. [CrossRef]

90. Chen, J.S.; Zhu, T.; Li, C.M.; Lou, X.W. Building hematite nanostructures by oriented attachment. *Angew. Chem. Int. Ed.* **2011**, *50*, 650–653. [CrossRef]

91. Ma, J.; Teo, J.; Mei, L.; Zhong, Z.; Li, Q.; Wang, T.; Duan, X.; Lian, J.; Zheng, W. Porous platelike hematite mesocrystals: Synthesis, catalytic and gas-sensing applications. *J. Mater. Chem.* **2012**, *22*, 11694–11700. [CrossRef]

92. Duan, X.; Mei, L.; Ma, J.; Li, Q.; Wang, T.; Zheng, W. Facet-induced formation of hematite mesocrystals with improved lithium storage properties. *Chem. Commun.* **2012**, *48*, 12204–12206. [CrossRef]

93. Fei, X.; Li, W.; Shao, Z.; Seeger, S.; Zhao, D.; Chen, X. Protein biomineralized nanoporous inorganic mesocrystals with tunable hierarchical nanostructures. *J. Am. Chem. Soc.* **2014**, *136*, 15781–15786. [CrossRef]

94. Cai, J.; Chen, S.; Ji, M.; Hu, J.; Ma, Y.; Qi, L. Organic additive-free synthesis of mesocrystalline hematite nanoplates via two-dimensional oriented attachment. *CrystEngComm* **2014**, *16*, 1553–1559. [CrossRef]

95. Agthe, M.; Plivelic, T.S.; Labrador, A.; Bergström, L.; Salazar-Alvarez, G. Following in real time the two-step assembly of nanoparticles into mesocrystals in levitating drops. *Nano Lett.* **2016**, *16*, 6838–6843. [CrossRef]

96. Liu, B.; Zeng, H.C. Mesoscale organization of CuO nanoribbons: Formation of "dandelions". *J. Am. Chem. Soc.* **2004**, *126*, 8124–8125. [CrossRef]

97. Yao, W.-T.; Yu, S.-H.; Zhou, Y.; Jiang, J.; Wu, Q.-S.; Zhang, L.; Jiang, J. Formation of uniform CuO nanorods by spontaneous aggregation: Selective synthesis of CuO, Cu$_2$O, and Cu nanoparticles by a solid-liquid phase arc discharge process. *J. Phys. Chem. B* **2005**, *109*, 14011–14016. [CrossRef]

98. Xu, M.; Wang, F.; Ding, B.; Song, X.; Fang, J. Electrochemical synthesis of leaf-like CuO mesocrystals and their lithium storage properties. *RSC Adv.* **2012**, *2*, 2240–2243. [CrossRef]

99. Jia, B.; Qin, M.; Zhang, Z.; Cao, Z.; Wu, H.; Chen, P.; Zhang, L.; Lu, X.; Qu, X. The formation of CuO porous mesocrystal ellipsoids via tuning the oriented attachment mechanism. *CrystEngComm* **2016**, *18*, 1376–1383. [CrossRef]

100. Zhang, J.; Cui, Y.; Qin, Q.; Zhang, G.; Luo, W.; Zheng, W. Nanoporous CuO mesocrystals: Low-temperature synthesis and improved structure-performance relationship for energy storage system. *Chem. Eng. J.* **2018**, *331*, 326–334. [CrossRef]

101. Hu, J.; Zou, C.; Su, Y.; Li, M.; Han, Y.; Kong, E.S.-W.; Yang, Z.; Zhang, Y. Ultrasensitive NO_2 gas sensor based on hierarchical Cu_2O/CuO mesocrystals nanoflower. *J. Mater. Chem. A* **2018**, *6*, 17120–17131. [CrossRef]

102. Zhao, J.; Tan, R.; Guo, Y.; Lu, Y.; Xu, W.; Song, W. SnO mesocrystals: Additive-free synthesis, oxidation, and top-down fabrication of quantum dots. *CrystEngComm* **2012**, *14*, 4575–4577. [CrossRef]

103. Chen, S.; Wang, M.; Ye, J.; Cai, J.; Ma, Y.; Zhou, H.; Qi, L. Kinetics-controlled growth of aligned mesocrystalline SnO_2 nanorod arrays for lithium-ion batteries with superior rate performance. *Nano Research* **2013**, *6*, 243–252. [CrossRef]

104. Liu, Y.; Zhu, G.; Ge, B.; Zhou, H.; Yuan, A.; Shen, X. Concave Co_3O_4 octahedral mesocrystal: Polymer-mediated synthesis and sensing properties. *CrystEngComm* **2012**, *14*, 6264–6270. [CrossRef]

105. Wang, F.; Lu, C.; Qin, Y.; Liang, C.; Zhao, M.; Yang, S.; Sun, Z.; Song, X. Solid state coalescence growth and electrochemical performance of plate-like Co_3O_4 mesocrystals as anode materials for lithium-ion batteries. *J. Power Sources* **2013**, *235*, 67–73. [CrossRef]

106. Su, D.; Dou, S.; Wang, G. Mesocrystal Co_3O_4 nanoplatelets as high capacity anode materials for Li-ion batteries. *Nano Res.* **2014**, *7*, 794–803. [CrossRef]

107. Hassen, D.; El-Safty, S.A.; Tsuchiya, K.; Chatterjee, A.; Elmarakbi, A.; Shenashen, M.A.; Sakai, M. Longitudinal hierarchy Co_3O_4 mesocrystals with high-dense exposure facets and anisotropic interfaces for direct-ethanol fuel cells. *Sci. Rep.* **2016**, *6*, 24330. [CrossRef]

108. Cao, W.; Wang, W.; Shi, H.; Wang, J.; Cao, M.; Liang, Y.; Zhu, M. Hierarchical three-dimensional flower-like Co_3O_4 architectures with a mesocrystal structure as high capacity anode materials for long-lived lithium-ion batteries. *Nano Res.* **2018**, *11*, 1437–1446. [CrossRef]

109. Fang, J.; Leufke, P.M.; Kruk, R.; Wang, D.; Scherer, T.; Hahn, H. External electric field driven 3D ordering architecture of silver (I) oxide meso-superstructures. *Nano Today* **2010**, *5*, 175–182. [CrossRef]

110. Belman, N.; Israelachvili, J.N.; Li, Y.; Safinya, C.R.; Ezersky, V.; Rabkin, A.; Sima, O.; Golan, Y. Hierarchical superstructure of alkylamine-coated ZnS nanoparticle assemblies. *Phys. Chem. Chem. Phys.* **2011**, *13*, 4974–4979. [CrossRef]

111. Querejeta-Fernandez, A.; Hernandez-Garrido, J.C.; Yang, H.; Zhou, Y.; Varela, A.; Parras, M.; Calvino-Gamez, J.J.; Gonzalez-Calbet, J.M.; Green, P.F.; Kotov, N.A. Unknown aspects of self-assembly of PbS microscale superstructures. *ACS Nano* **2012**, *6*, 3800–3812. [CrossRef]

112. Simon, P.; Rosseeva, E.; Baburin, I.A.; Liebscher, L.; Hickey, S.G.; Cardoso-Gil, R.; Eychmüller, A.; Kniep, R.; Carrillo-Cabrera, W. PbS-organic mesocrystals: The relationship between nanocrystal orientation and superlattice array. *Angew. Chem. Int. Ed.* **2012**, *51*, 10776–10781. [CrossRef]

113. Simon, P.; Bahrig, L.; Baburin, I.A.; Formanek, P.; Röder, F.; Sickmann, J.; Hickey, S.G.; Eychmüller, A.; Lichte, H.; Kniep, R.; et al. Interconnection of nanoparticles within 2D superlattices of PbS/oleic acid thin films. *Adv. Mater.* **2014**, *26*, 3042–3049. [CrossRef]

114. De la Rica, R.; Velders, A.H. Biomimetic crystallization of Ag_2S nanoclusters in nanopore assemblies. *J. Am. Chem. Soc.* **2011**, *133*, 2875–2877. [CrossRef] [PubMed]

115. Nagaoka, Y.; Chen, O.; Wang, Z.; Cao, Y.C. Structural control of nanocrystal superlattices using organic guest molecules. *J. Am. Chem. Soc.* **2012**, *134*, 2868–2871. [CrossRef] [PubMed]

116. Soejima, T.; Kimizuka, N. One-pot room-temperature synthesis of single-crystalline gold nanocorolla in water. *J. Am. Chem. Soc.* **2009**, *131*, 14407–14412. [CrossRef]

117. Fang, J.; Du, S.; Lebedkin, S.; Li, Z.; Kruk, R.; Kappes, M.; Hahn, H. Gold mesostructures with tailored surface topography and their self-assembly arrays for surface-enhanced raman spectroscopy. *Nano Lett.* **2010**, *10*, 5006–5013. [CrossRef]

118. You, H.; Ji, Y.; Wang, L.; Yang, S.; Yang, Z.; Fang, J.; Song, X.; Ding, B. Interface synthesis of gold mesocrystals with highly roughened surfaces for surface-enhanced Raman spectroscopy. *J. Mater. Chem.* **2012**, *22*, 1998–2006. [CrossRef]

119. Fang, J.; Ding, B.; Song, X. Self-assembly mechanism of platelike silver mesocrystal. *Appl. Phys. Lett.* **2007**, *91*, 083108. [CrossRef]

120. Cao, Y.; Fan, J.; Bai, L.; Hu, P.; Yang, G.; Yuan, F.; Chen, Y. Formation of cubic Cu mesocrystals by a solvothermal reaction. *CrystEngComm* **2010**, *12*, 3894–3899. [CrossRef]

121. Li, T.; You, H.; Xu, M.; Song, X.; Fang, J. Electrocatalytic properties of hollow coral-like platinum mesocrystals. *ACS Appl. Mater. Interfaces* **2012**, *4*, 6942–6948. [CrossRef]

122. Zhong, P.; Liu, H.; Zhang, J.; Yin, Y.; Gao, C. Controlled Synthesis of octahedral platinum-based mesocrystals by oriented aggregation. *Chem. Eur. J.* **2017**, *23*, 6803–6810. [CrossRef] [PubMed]

123. Huang, X.; Tang, S.; Yang, J.; Tan, Y.; Zheng, N. Etching growth under surface confinement: An effective strategy to prepare mesocrystalline Pd nanocorolla. *J. Am. Chem. Soc.* **2011**, *133*, 15946–15949. [CrossRef] [PubMed]

124. Cai, J.; Qi, L. TiO$_2$ mesocrystals: Synthesis, formation mechanisms and applications. *Sci. China Chem.* **2012**, *55*, 2318–2326. [CrossRef]

125. Hong, Z.; Wei, M. Recent progress in preparation and lithium-ion storage properties of TiO$_2$ mesocrystals. *J. Chin. Chem. Soc.* **2015**, *62*, 209–216. [CrossRef]

126. Zhang, P.; Tachikawa, T.; Fujitsuka, M.; Majima, T. The development of functional mesocrystals for energy harvesting, storage, and conversion. *Chem. Eur. J.* **2018**, *24*, 6295–6307. [CrossRef]

127. Li, L.; Liu, C.-Y. Organic small molecule-assisted synthesis of high active TiO$_2$ rod-like mesocrystals. *CrystEngComm* **2010**, *12*, 2073–2078. [CrossRef]

128. Zhang, D.; Li, G.; Wang, F.; Yu, J.C. Green synthesis of a self-assembled rutile mesocrystalline photocatalyst. *CrystEngComm* **2010**, *12*, 1759–1763. [CrossRef]

129. Liu, X.; Gao, Y.; Cao, C.; Luo, H.; Wang, W. Highly crystalline spindle-shaped mesoporous anatase titania particles: Solution-phase synthesis, characterization, and photocatalytic properties. *Langmuir* **2010**, *26*, 7671–7674. [CrossRef]

130. Bian, Z.; Zhu, J.; Wen, J.; Cao, F.; Huo, Y.; Qian, X.; Cao, Y.; Shen, M.; Li, H.; Lu, Y. Single-crystal-like titania mesocages. *Angew. Chem. Int. Ed.* **2011**, *123*, 1137–1140. [CrossRef]

131. Da Silva, R.O.; Gonçalves, R.H.; Stroppa, D.G.; Ramirez, A.J.; Leite, E.R. Synthesis of recrystallized anatase TiO$_2$ mesocrystals with Wulff shape assisted by oriented attachment. *Nanoscale* **2011**, *3*, 1910–1916. [CrossRef]

132. Tartaj, P. Sub-100 nm TiO$_2$ mesocrystalline assemblies with mesopores: Preparation, characterization, enzyme immobilization and photocatalytic properties. *Chem. Commun.* **2011**, *47*, 256–258. [CrossRef]

133. Tartaj, P.; Amarilla, J.M. Multifunctional response of anatase nanostructures based on 25 nm mesocrystal-like porous assemblies. *Adv. Mater.* **2011**, *23*, 4904–4907. [CrossRef]

134. Jiao, W.; Wang, L.; Liu, G.; Lu, G.Q.; Cheng, H.-M. Hollow anatase TiO$_2$ single crystals and mesocrystals with dominant {101} facets for improved photocatalysis activity and tuned reaction preference. *ACS Catal.* **2012**, *2*, 1854–1859. [CrossRef]

135. Bian, Z.; Tachikawa, T.; Majima, T. Superstructure of TiO$_2$ crystalline nanoparticles yields effective conduction pathways for photogenerated charges. *J. Phys. Chem. Lett.* **2012**, *3*, 1422–1427. [CrossRef]

136. Chen, Q.; Ma, W.; Chen, C.; Ji, H.; Zhao, J. Anatase TiO$_2$ mesocrystals enclosed by (001) and (101) facets: Synergistic effects between Ti^{3+} and facets for their photocatalytic performance. *Chem. Eur. J.* **2012**, *18*, 12584–12589. [CrossRef]

137. Liu, Y.; Zhang, Y.; Li, H.; Wang, J. Manipulating the formation of NH$_4$TiOF$_3$ mesocrystals: Effects of temperature, surfactant, and pH. *Cryst. Growth Des.* **2012**, *12*, 2625–2633. [CrossRef]

138. Aoyama, Y.; Oaki, Y.; Ise, R.; Imai, H. Mesocrystal nanosheet of rutile TiO$_2$ and its reaction selectivity as a photocatalyst. *CrystEngComm* **2012**, *14*, 1405–1411. [CrossRef]

139. Zhou, L.; Chen, J.; Ji, C.; Zhou, L.; O'Brien, P. A facile solid phase reaction to prepare TiO$_2$ mesocrystals with exposed {001} facets and high photocatalytic activity. *CrystEngComm* **2013**, *15*, 5012–5015. [CrossRef]

140. Yao, X.; Liu, X.; Liu, T.; Wang, K.; Lu, L. One-step and large-scale synthesis of anatase TiO$_2$ mesocrystals along [001] orientation with enhanced photocatalytic performance. *CrystEngComm* **2013**, *15*, 10246–10254. [CrossRef]

141. Guo, Y.; Li, H.; Chen, J.; Wu, X.; Zhou, L. TiO$_2$ mesocrystals built of nanocrystals with exposed {001} facets: Facile synthesis and superior photocatalytic ability. *J. Mater. Chem. A* **2014**, *2*, 19589–19593. [CrossRef]

142. Chen, J.; Li, G.; Zhang, H.; Liu, P.; Zhao, H.; An, T. Anatase TiO$_2$ mesocrystals with exposed (001) surface for enhanced photocatalytic decomposition capability toward gaseous styrene. *Catal. Today* **2014**, *224*, 216–224. [CrossRef]

143. Fang, Z.; Long, L.; Hao, S.; Song, Y.; Qiang, T.; Geng, B. Mesocrystal precursor transformation strategy for synthesizing ordered hierarchical hollow TiO$_2$ nanobricks with enhanced photocatalytic property. *CrystEngComm* **2014**, *16*, 2061–2069. [CrossRef]

144. Lai, L.-L.; Huang, L.-L.; Wu, J.-M. K$_2$TiO(C$_2$O$_4$)$_2$-mediated synthesis of rutile TiO$_2$ mesocrystals and their ability to assist photodegradation of sulfosalicylic acid in water. *RSC Adv.* **2014**, *4*, 49280–49286. [CrossRef]

145. Zhang, P.; Tachikawa, T.; Bian, Z.; Majima, T. Selective photoredox activity on specific facet-dominated TiO$_2$ mesocrystal superstructures incubated with directed nanocrystals. *Appl. Catal. B* **2015**, *176–177*, 678–686. [CrossRef]

146. Hu, D.; Zhang, W.; Tanaka, Y.; Kusunose, N.; Peng, Y.; Feng, Q. Mesocrystalline nanocomposites of TiO$_2$ polymorphs: Topochemical mesocrystal conversion, characterization, and photocatalytic response. *Cryst. Growth Des.* **2015**, *15*, 1214–1225. [CrossRef]

147. Fu, X.X.; Ren, Z.M.; Fan, C.Y.; Sun, C.X.; Shi, L.; Yu, S.Q.; Qian, G.D.; Wang, Z.Y. Designed fabrication of anatase mesocrystals constructed from crystallographically oriented nanocrystals for improved photocatalytic activity. *RSC Adv.* **2015**, *5*, 41218–41223. [CrossRef]

148. Lai, L.-L.; Wu, J.-M. Hollow TiO$_2$ microspheres assembled with rutile mesocrystals: Low-temperature one-pot synthesis and the photocatalytic performance. *Ceram. Int.* **2015**, *41*, 12317–12322. [CrossRef]

149. Fu, X.; Fan, C.; Yu, S.; Shi, L.; Wang, Z. TiO$_2$ mesocrystals with exposed {001} facets as efficient photocatalysts. *J. Alloys Compd.* **2016**, *680*, 80–86. [CrossRef]

150. Tan, B.; Zhang, X.; Li, Y.; Chen, H.; Ye, X.; Wang, Y.; Ye, J. Anatase TiO$_2$ mesocrystals: Green synthesis, in situ conversion to porous single crystals, and self-doping Ti^{3+} for enhanced visible light driven photocatalytic removal of NO. *Chem. Eur. J.* **2017**, *23*, 5478–5487. [CrossRef]

151. Tang, C.; Liu, L.; Li, Y.; Bian, Z. Aerosol spray assisted assembly of TiO$_2$ mesocrystals into hierarchical hollow microspheres with enhanced photocatalytic performance. *Appl. Catal. B* **2017**, *201*, 41–47. [CrossRef]

152. Wang, H.; Chen, Q.; Luan, Q.; Duan, R.; Guan, R.; Cao, X.; Hu, X. Photocatalytic properties dependent on the interfacial defects of intergrains within TiO$_2$ mesocrystals. *Chem. Eur. J.* **2018**, *24*, 17105–17116. [CrossRef] [PubMed]

153. Hong, Z.; Dai, H.; Huang, Z.; Wei, M. Understanding the growth and photoelectrochemical properties of mesocrystals and single crystals: A case of anatase TiO$_2$. *Phys. Chem. Chem. Phys.* **2014**, *16*, 7441–7447. [CrossRef] [PubMed]

154. Zhang, Y.; Cai, J.; Ma, Y.; Qi, L. Mesocrystalline TiO$_2$ nanosheet arrays with exposed {001} facets: Synthesis via topotactic transformation and applications in dye-sensitized solar cells. *Nano Res.* **2017**, *10*, 2610–2625. [CrossRef]

155. Liu, B.; Zeng, H.C. Carbon nanotubes supported mesoporous mesocrystals of anatase TiO$_2$. *Chem. Mater.* **2008**, *20*, 2711–2718. [CrossRef]

156. Li, N.; Liu, G.; Zhen, C.; Li, F.; Zhang, L.; Cheng, H.-M. Battery performance and photocatalytic activity of mesoporous anatase TiO$_2$ nanospheres/graphene composites by template-free self-assembly. *Adv. Funct. Mater.* **2011**, *21*, 1717–1722. [CrossRef]

157. Zhang, W.; Shen, D.; Liu, Z.; Wu, N.-L.; Wei, M. Brookite TiO$_2$ mesocrystals with enhanced lithium-ion intercalation properties. *Chem. Commun.* **2018**, *54*, 11491–11494. [CrossRef]

158. Elbanna, O.; Zhang, P.; Fujitsuka, M.; Majima, T. Facile preparation of nitrogen and fluorine codoped TiO$_2$ mesocrystal with visible light photocatalytic activity. *Appl. Catal. B* **2016**, *192*, 80–87. [CrossRef]

159. Zhang, P.; Fujitsuka, M.; Majima, T. TiO$_2$ mesocrystal with nitrogen and fluorine codoping during topochemical transformation: Efficient visible light induced photocatalyst with the codopants. *Appl. Catal. B* **2016**, *185*, 181–188. [CrossRef]

160. Primc, D.; Niederberger, M. Synthesis and formation mechanism of multicomponent Sb-Nb:TiO$_2$ mesocrystals. *Chem. Mater.* **2017**, *29*, 10113–10121. [CrossRef]

161. Lan, T.; Zhang, W.; Wu, N.-L.; Wei, M. Nb-doped rutile TiO$_2$ mesocrystals with enhanced lithium storage properties for lithium ion battery. *Chem. Eur. J.* **2017**, *23*, 5059–5065. [CrossRef]

162. Naldoni, A.; Allieta, M.; Santangelo, S.; Marelli, M.; Fabbri, F.; Cappelli, S.; Bianchi, C.L.; Psaro, R.; Santo, V.D. Effect of nature and location of defects on bandgap narrowing in black TiO_2 nanoparticles. *J. Am. Chem. Soc.* **2012**, *134*, 7600–7603. [CrossRef] [PubMed]

163. Pan, X.; Yang, M.-Q.; Fu, X.; Zhang, N.; Xu, Y.-J. Defective TiO_2 with oxygen vacancies: Synthesis, properties and photocatalytic applications. *Nanoscale* **2013**, *5*, 3601–3614. [CrossRef] [PubMed]

164. Chen, X.; Liu, L.; Huang, F. Black titanium dioxide (TiO_2) nanomaterials. *Chem. Soc. Rev.* **2015**, *44*, 1861–1885. [CrossRef]

165. Ullattil, S.G.; Narendranath, S.B.; Pillai, S.C.; Periyat, P. Black TiO_2 nanomaterials: A review of recent advances. *Chem. Eng. J.* **2018**, *343*, 708–736. [CrossRef]

166. Zhou, W.; Fu, H. Defect-mediated electron-hole separation in semiconductor photocatalysis. *Inorg. Chem. Front.* **2018**, *5*, 1240–1254. [CrossRef]

167. Chen, X.; Liu, L.; Yu, P.Y.; Mao, S.S. Increasing solar absorption for photocatalysis with black hydrogenated titanium dioxide nanocrystals. *Science* **2011**, *331*, 746–750. [CrossRef] [PubMed]

168. Elbanna, O.; Fujitsuka, M.; Kim, S.; Majima, T. Charge carrier dynamics in TiO_2 mesocrystals with oxygen vacancies for photocatalytic hydrogen generation under solar light irradiation. *J. Phys. Chem. C* **2018**, *122*, 15163–15170. [CrossRef]

169. Bian, Z.; Tachikawa, T.; Kim, W.; Choi, W.; Majima, T. Superior electron transport and photocatalytic abilities of metal-nanoparticle-loaded TiO_2 superstructures. *J. Phys. Chem. C* **2012**, *116*, 25444–25453. [CrossRef]

170. Gao, P.; Liu, J.; Zhang, T.; Sun, D.D.; Ng, W. Hierarchical TiO_2/CdS "spindle-like" composite with high photodegradation and antibacterial capability under visible light irradiation. *J. Hazard. Mater.* **2012**, *229–230*, 209–216. [CrossRef]

171. Yang, X.; Qin, J.; Li, Y.; Zhang, R.; Tang, H. Graphene-spindle shaped TiO_2 mesocrystal composites: Facile synthesis and enhanced visible light photocatalytic performance. *J. Hazard. Mater.* **2013**, *261*, 342–350. [CrossRef]

172. Bian, Z.; Tachikawa, T.; Zhang, P.; Fujitsuka, M.; Majima, T. Au/TiO_2 superstructure-based plasmonic photocatalysts exhibiting efficient charge separation and unprecedented activity. *J. Am. Chem. Soc.* **2014**, *136*, 458–465. [CrossRef] [PubMed]

173. Tachikawa, T.; Zhang, P.; Bian, Z.; Majima, T. Efficient charge separation and photooxidation on cobalt phosphate-loaded TiO_2 mesocrystal superstructures. *J. Mater. Chem. A* **2014**, *2*, 3381–3388. [CrossRef]

174. Zhang, P.; Tachikawa, T.; Fujitsuka, M.; Majima, T. Efficient charge separation on 3D architectures of TiO_2 mesocrystals packed with a chemically exfoliated MoS_2 shell in synergetic hydrogen evolution. *Chem. Commun.* **2015**, *51*, 7187–7190. [CrossRef]

175. Li, X.; Wang, J.; Men, Y.; Bian, Z. TiO_2 mesocrystal with exposed (001) facets and CdS quantum dots as an active visible photocatalyst for selective oxidation reactions. *Appl. Catal. B* **2016**, *187*, 115–121. [CrossRef]

176. Han, T.; Wang, H.; Zheng, X. Gold nanoparticle incorporation into nanoporous anatase TiO_2 mesocrystal using a simple deposition-precipitation method for photocatalytic applications. *RSC Adv.* **2016**, *6*, 7829–7837. [CrossRef]

177. Yan, D.; Liu, Y.; Liu, C.-Y.; Zhang, Z.-Y.; Niea, S.-D. Multi-component in situ and in-step formation of visible-light response C-dots composite TiO_2 mesocrystals. *RSC Adv.* **2016**, *6*, 14306–14313. [CrossRef]

178. Tang, H.; Chang, S.; Jiang, L.; Tang, G.; Liang, W. Novel spindle-shaped nanoporous TiO_2 coupled graphitic g-C_3N_4 nanosheets with enhanced visible-light photocatalytic activity. *Ceram. Int.* **2016**, *42*, 18443–18452. [CrossRef]

179. Elbanna, O.; Kim, S.; Fujitsuka, M.; Majima, T. TiO_2 mesocrystals composited with gold nanorods for highly efficient visible-NIR-photocatalytic hydrogen production. *Nano Energy* **2017**, *35*, 1–8. [CrossRef]

180. Elbanna, O.; Fujitsuka, M.; Majima, T. g-C_3N_4/TiO_2 mesocrystals composite for H_2 evolution under visible-light irradiation and its charge carrier dynamics. *ACS Appl. Mater. Interfaces* **2017**, *9*, 34844–34854. [CrossRef]

181. Yu, X.; Fan, X.; An, L.; Liu, G.; Li, Z.; Liu, J.; Hu, P.A. Mesocrystalline Ti^{3+}-TiO_2 hybridized g-C_3N_4 for efficient visible-light photocatalysis. *Carbon* **2018**, *128*, 21–30. [CrossRef]

182. Xue, J.; Elbanna, O.; Kim, S.; Fujitsuka, M.; Majima, T. Defect state-induced efficient hot electron transfer in Au nanoparticles/reduced TiO_2 mesocrystal photocatalysts. *Chem. Commun.* **2018**, *54*, 6052–6055. [CrossRef]

183. Tan, B.; Ye, X.; Li, Y.; Ma, X.; Wang, Y.; Ye, J. Defective anatase TiO_{2-x} mesocrystal growth in situ on g-C_3N_4 nanosheets: Construction of 3D/2D Z-scheme heterostructures for highly efficient visible-light photocatalysis. *Chem. Eur. J.* **2018**, *24*, 13311–13321. [CrossRef]
184. Chen, F.; Cao, F.; Li, H.; Bian, Z. Exploring the important role of nanocrystals orientation in TiO_2 superstructure on photocatalytic performances. *Langmuir* **2015**, *31*, 3494–3499. [CrossRef]